Icephobic Surfaces: Definition and Figures of

Merit

Peyman Irajizad, Sina Nazifi, and Hadi Ghasemi*

Department of Mechanical Engineering, University of Houston, 4726 Calhoun Rd, Houston,

Texas, 77204-4006, USA

E-mail: hghasemi@uh.edu

Keywords: (icephobic, ice nucleation, ice growth, ice adhesion, and durability)

Abstract

Icephobic surfaces have a critical footprint on human daily lives ranging from aviation systems

and infrastructures to energy systems, but creation of these surfaces for low-temperature

applications remains elusive. Non-wetting, liquid-infused and hydrated surfaces have inspired

routes for development of icephobic surfaces. However, high freezing temperature, high ice

adhesion strength and subsequent ice accretion, low mechanical durability, and high production

cost have restricted their practical applications. In this review, we provide a comprehensive

definition for icephobicity through thermodynamics, heat transfer and mechanics of ice/water-

material interface and elucidate physic-based routes through which nano-scale could help to

achieve exceptional icephobic surfaces. Based on conservation laws, mathematical models are

developed that accurately predict ice growth rate on various substrates and wind conditions.

Through physics of fracture at ice-icephobic material interface, we cast a standard method for ice

1

adhesion measurement that has the potential to eliminate discrepancies between reported ice adhesion from different laboratories. To assure long-time performance of icephobic surfaces, durability metrics need to be defined. We provide standard methods to examine mechanical, chemical, and environmental durability of icephobic surfaces. In the developed comprehensive framework on icephobicity in this review, performance of state-of-the-art icephobic surfaces are compared and main deficiencies in this field are highlighted.

1. Introduction

Icing is an omnipresent phenomenon in subzero climates where water and/or moisture are present [1–3], and it impacts a broad spectrum of industries ranging from transportation systems[4–6], power transmission lines[7], and infrastructures[8,9] to energy systems[10–14], Fig. 1. Icing in aircrafts results in increased drag and may lead to loss of lift force and potential catastrophic events. Icing in electricity transmission systems can lead to collapse of poles and towers and rupture of conductors. Icing in cooling systems significantly drops the heat transfer rate leading to their inefficient operation. According to Lawrence Berkeley Laboratory, ice storms account for 10% of power transmission outages in US [15,16]. The financial market for icephobic surfaces is approximately \$20 billion (B) annually[17] including \$10.17 B Aerospace, \$3 B Automobile, \$2.3 B infrastructures, \$3-5 B power transmission lines. In addition to these markets, there is a significant market for icephobic surfaces in coastguards and shipping industries. Rather than economical role, icing problem has a critical footprint on daily human life living in cold climates. Around 3 million people every winter in US suffer from power losses caused by ice storms.

Despite its vital role in economy and society, development of durable and high-performance icephobic surfaces remains a challenge. The main figures of merit for icephobic surfaces are low

freezing temperature, low ice accretion rate, low ice adhesion and long-term durability. The required figures of merit depend on the type of application for icephobic surfaces. For example, for aircrafts, low freezing temperature, low ice adhesion and durability are the most critical figures of merit. Over decades, a range of surfaces (e.g. superhydrophobic[18-60], liquidinfused[20,61] and hydrated surfaces[62]) are developed to meet these criteria. Despite significant progress, development of surfaces to address all the required figures of merit remain a challenge. A rational strategy for development of disruptive icephobic surfaces requires a fundamental understanding of physics of ice formation, ice growth and adhesion at the solid-ice interface and the dependence of these physics on the length scale. Thermodynamics of phase change at the solid-water interface governs the freezing temperature, heat transfer governs the ice growth, and the interfacial mechanics govern the ice adhesion at the interface. A comprehensive body of knowledge on these physics allows to cast a set of criteria to assess icephobic surfaces and to rationally develop new icephobic surfaces. We should add that physics of frost nucleation and growth differs from that of ice and is not discussed here. The readers may refer to the cited articles [28,63–71].

2. Definition of icephobicity

Sometimes icephobicity of a surface is assessed through either single or multiple material characteristics including water repellency or contact angle hysteresis. Although these characteristics may indirectly affect icephobicity of a surface, strictly speaking, they are not direct measures of icephobic characteristics of a surface. A range of studies in the literature directly correlated the water repellency to icephobicity. Dalton et al. [72] developed a range of surfaces ranging from superhydrophilic surfaces to superhydrophobic surfaces. They found that ice adhesion decreases as contact angle of water on surfaces increases. They reported 18-fold

reduction in ice adhesion on the most superhydrophobic surface compared to untreated aluminum surface. Kulinich et al.[48] reported that the correlation between ice adhesion and contact angle is only valid when contact angle hysteresis is low. They suggested that the icephobicity is correlated with contact angle hysteresis. That is, higher contact angle hysteresis indicated higher ice-solid surface area consequently higher ice adhesion. Cao et al.[73] developed a range of nanoparticles-polymer composites to explore the correlation between icephobicity and superhydrophobicity. They found that the icephobicity depends on both hydrophobicity and also dimension of particles exposed to the surface (i.e. surface morphology). Meuler et al.[22] studied ice adhesion on a wide range of smooth steel discs coated with various hydrophobic coatings. They suggested that ice adhesion is correlated to the value of work of adhesion (i.e. $W_a = \sigma^{LV}(1 + \cos \theta_r)$) and further reduction in ice adhesion is possible only through structured surfaces. In a following work, Meuler et al.[21] suggested that superhydrophobic surfaces could repel impinging water drops before freezing resulting to icephobicity. Zheng et al. [74] also showed that on carbon-nanotube based superhydrophobic surfaces, water drops repellency before freezing helps to have icephobic properties. Jung et al.[75] demonstrated that for superhydrophobic surfaces, high contact angle increases the delay time for ice formation. However, for hydrophilic surfaces, smoother surface provides higher delay time in ice formation. That is for design of icephobic surfaces, competing effects of wettability and roughness should be optimized. Kulinich et al.[57] suggested that although superhydrophobic surfaces may show icephobicity in laboratory conditions, in humid atmosphere their anti-icing efficiency drops significantly. In humid atmosphere, water condenses both on top and between surfaces asperities and increase ice adhesion strength. Furthermore, they raised a concern on durability of superhydrophobic surfaces in which after few icing/deicing

cycles, icephobicity of superhydrophobic surfaces deteriorate and surface asperities are gradually damaged. Bahadur et al.[37] modeled the ice formation on superhydrophobic surfaces and suggested that these surfaces can prevent freezing of impacting droplets up to temperature of -20 to -25 °C. Despite these early demonstrations on icephobicity of superhydrophobic surfaces, Nosonovsky and Hejazi[76] argued that superhydrophobicity does not have a direct correlation with icephobicity. The mechanics of ice and water adhesion on a surface are different. Although, water can withstand positive and negative pressures, it cannot support shear stress. A drop under shear stress deforms and de-wets the surface once the shear force is more than counteract force by the contact angle hysteresis. However, the scenario is different when the drops freeze. Ice can withstand shear and detachment of ice from a surface occurs through fracture. The shear stress for fracture depends on the work of adhesion on a surface (i.e. W_a) and the initial dimension of crack. The work of adhesion is correlated to receding contact angle. This is the reason for superhydrophobic surfaces to show low ice adhesion. However, the dimension of crack (i.e. void) at the interface is critical for fracture. Even for high values of receding contact angle, the dimension of voids at the interface is a critical parameter for icephobicity. Thus, a thorough definition of icephobicity is required that addresses all these effects.

A comprehensive icephobicity definition includes four physics: physic (I) governed by thermodynamics of phase change of supercooled water-surface system, physic (II) governed by heat transfer in the ice formation process, physic (III) governed by mechanics of the ice-surface system, and physic (IV) governed by material characteristics for long-term mechanical, chemical and environmental durability. All these physics play critical roles in the icephobicity of a surface. According to this definition, icephobic surfaces are characterized with four main figures of merit: (1) median ice nucleation temperature, T_N defined as ice nucleation temperature of a sessile

water droplet placed on a surface when the system of droplet, surface and surrounding is cooled in a slow and quasi-equilibrium approach **or** average ice nucleation delay time, τ_{av} , defined as the average time required for ice nucleation of a super-cooled droplet on a surface in thermal equilibrium with its surrounding[75,77], (2) ice accretion rate on a surface, (3) adhesion strength at the ice-solid interface, and (4) long-term icephobicity of a surface.

3. Ice nucleation on a surface

Once a water droplet contacts a subzero surface, phase transformation of water to ice can occur through nucleation of ice and further growth. From a thermodynamic perspective, ice nucleation temperature, T_N (see Appendix A for definition and measurement approach), is a function of Gibbs energy barrier for heterogeneous ice nucleation (ΔG^*) written as [78]

$$\Delta G^* = \frac{16 \pi \gamma_{IW}^3}{3 \Delta G_n^2} f(m, x)$$
 (1)

where γ_{IW} denotes the interfacial tension of water-ice nucleolus, ΔG_v the volumetric free energy of phase-change and f(m,x) is the surface factor, which is governed by the energy and geometry of the involved interfaces. The value of f(m,x) varies between 0 and 1, in which 1 corresponds to homogenous nucleation limit (no involved surfaces) and 0 correspond to ice nucleation with no sub-cooling. In function f(m,x), value of m depends on surface energy of the interfaces ($m = \cos \theta = (\gamma_{SW} - \gamma_{SI})/\gamma_{WI}$), where γ_{SW} denotes the surface energy of solid-water interface, γ_{SI} the surface energy of solid-ice interface, and γ_{WI} the surface energy of water-ice interface, Fig. 2a. Also, the value of $x = \frac{R}{r_c}$ depends on the radius of features at the surface (R), and the critical nucleolus radius (r_c), which is equal to $\frac{2\gamma_{IW}}{\Delta G_v}$. The functional form of f(m,x) for convex and concave surface are derived by Fletcher et al.[78] and is written as

For convex surfaces

$$f(m,x) = \frac{1}{2} \left\{ 1 + \left(\frac{1 - mx}{g_v} \right)^3 + x^3 \left[2 - 3 \left(\frac{x - m}{g_v} \right) + \left(\frac{x - m}{g_v} \right)^3 \right] + 3mx^2 \left(\frac{x - m}{g_v} - 1 \right) \right\}$$

$$g_v = (1 + x^2 - 2mx)^{1/2}$$
(2)

And for concave surfaces

$$f(m,x) = \frac{1}{2} \left\{ 1 - \left(\frac{1+mx}{g_c} \right)^3 - x^3 \left[2 - 3 \left(\frac{x+m}{g_c} \right) + \left(\frac{x+m}{g_c} \right)^3 \right] + 3mx^2 \left(\frac{x+m}{g_c} - 1 \right) \right\}$$

$$g_c = (1+x^2+2mx)^{1/2}$$
(3)

We plotted these functions for both convex and concave surfaces in **Fig. 2**. As shown, for a given value of m (i.e. solid surface), f(m,x) function becomes independent of x, unless the value of the x is in the range of 0-10. That is, radius of features on the surface should be in order of critical nucleolus radius, which varies from 1.53-4.74 nm for a temperature range of -30 to -10 $^{\circ}$ C (see Appendix B). Note that value of f goes to zero if m = 1 and m > 1 (i.e. no sub-cooling scenario). For the value of m = 1 to be equal to 1, the solid-water-ice system should satisfy the following condition: $\gamma_{SW} \ge \gamma_{SI} + \gamma_{WI}$. And for rough surfaces, the condition of m = 1 and m > 1 is satisfied. For the value of m = 1 and m > 1, m > 1 value becomes smaller than one. That is, nano-scale confinement leads to suppression of ice nucleation.

For a given solid with a specific surface energy and roughness, if the value of x is smaller than \sim 1, roughness affects ice nucleation. However, if the value of x is greater than 1, ice nucleation is independent of surface structuring (i.e. micro/nano). This fact is also discussed by Eberle et al.[77]. They showed that ice nucleation temperature (T_N) is unaffected unless radius of curvature is < 10 nm. Furthermore, through molecular dynamic simulations, Li et al[79] showed that nano-grooves could reduce ice nucleation rate ($1/\tau_{av}$) and suppress freezing. Thus, for most

of the micro/nano-structured surfaces (i.e. roughness in order of >10 nm), the route to increase energy barrier for ice nucleation is through m parameter (i.e. tuning of surface energies). In function, m, as γ_{IW} is only a function of temperature (see Appendix B), the governing interfacial property becomes $(\gamma_{Sw} - \gamma_{SI})$. Note that the differential of these surfaces energies is important in the ice nucleation and not the individual surface energies. Studies have been mostly focused to reduce the value of γ_{Sa} through perfluorinated groups (-CF2 or -CF3), where subscript Sadenotes solid-air interface. The lowest achieved surface energy is through a mono-layer of -CF₃ group $(\gamma_{Sa} \approx 6 - 10 \, mN/m)$.[80] Through grafting of perfluorodecyltrichlorosilane (FDTS) monolayer on a surface, Eberle et al. [77] achieved contact angle of 100° for ice-water nucleolus and m value of - 0.17. As radii of curvature on these developed surfaces was well above critical nucleolus size (i.e. $x \gg 1$), curvature did not affect surface factor and f(m, x) = 0.57. Furthermore, these authors suggested that formation of quasiliquid layer underneath of ice nucleolus affect the value of m in local nanoconfined geometries. They provided a correlation to determine the revised value of m which has dependence on radius of curvature of local confinements. Irajizad et al. [81-83] took another approach to reduce the value of m by introduction of magnetic slippery surfaces (MAGSS). In these surfaces, volumetric magnetic force is exploited to form a liquid-liquid surface. They tuned the differential value of $(\gamma_{SW} - \gamma_{SI})$ through introduction of a selective ferrofluid on a surface. Through concept of magnetic liquid surfaces, the authors achieved the value of m = -0.95, which corresponds to value of 0.98 for f(m,x). Note that the homogenous limit of ice nucleation corresponds to f(m,x) equal to 1. Thus, through rational modification of interfacial surface energies and roughness of a surface, one can boost the energy barrier for ice nucleation (i.e. f(m, x)) and consequently decrease ice nucleation temperature.

Another thermodynamic aspect of ice formation is ice nucleation delay time (τ_{av}) or the nucleation rate. In the classical nucleation theory[78,84,85], nucleation rate, I(T), is given by

$$\tau_{av}^{-1} = J(T) = K \exp\left(-\frac{\Delta G^*}{k_B T}\right)$$
(4)

where K is the kinetic constant and k_B is the Boltzmann constant. Kinetic constant $(K = Z\beta N)$ depends on number of atomic nucleation sites per unit volume (N), Zeldovich non-equilibrium factor (Z), and rate at which atoms or molecules are added to the critical nucleus (β)[84]. The dependence of K on material properties remains to be an open question. As discussed in Eq. 1, the value of ΔG^* is mainly governed by function f(m,x), which is a surface factor. Thus, to fundamentally tune the ice nucleation rate, one should actuate the interfacial energies and surface structuring in few nanometers scale. For example, Tourkine et al. [52] used superhydrophobic surfaces to increase ice nucleation delay time. Through grafting of fluorinated thiols on a rough copper substrate, they developed superhydrophobic surfaces. They showed that ice nucleation delay time is an order of magnitude higher on superhydrophobic surfaces compared to flat surfaces. Alizadeh et al. [24] showed that, under low humidity condition, ice nucleation delay time is boosted through both surface chemistry and roughness. They developed superhydrophobic surfaces through grafting of tridecafluoro-1,1,2,2-tetrahydrooctyl trichlorosilane on nanostructures silicon surfaces. The role of superhydrophobicity on boosting the ice nucleation delay time is also discussed by Oberli et al. [33]. They suggested higher contact angle of droplet on a surface corresponded higher time delay in ice nucleation.

Although the classical picture of ice nucleation provides a rational route to achieve exceptional icephobic surfaces, an assumption is hidden in this formulation, which may not be valid at nanoscale. We can rewrite the rate of nucleation in terms of chemical potential,

$$J(T) = K \exp\left(\frac{-8\pi\gamma_{IW}^3}{3k_bT(\rho\Delta\mu)^2}\right)$$
 (5)

where ρ denotes the molar density of liquid and $\Delta\mu$ the chemical potential difference between the water and ice phases. The difference in chemical potential depends on the thermodynamic state of the system (both temperature and pressure of the system). For an isothermal system, the functional form of chemical potential is written as

$$\Delta\mu (T, P) = \Delta\mu (T, P_{atm}) + (P_L - P_{atm}) (v_w - v_i)$$
(6)

Where P_L denotes the liquid pressure, P_{atm} denotes atmospheric pressure, and v_w and v_i are the specific volume of liquid and ice phases. For a droplet, the liquid pressure is governed by Laplace equation (i.e. $P_L - P_{atm} = 2\gamma_{LV}/r$), where γ_{LV} is the liquid-vapor surface tension and r is the mean radius of curvature. This equation is valid down to few nm as shown by several studies [86–88]. At macro-scale, due to large radius of curvature, the liquid pressure is close to atmospheric pressure and the last term is negligible compared to the other terms. However, this term becomes significant at nano-scale. If the last term in Eq. 6 is positive, the pressure will enhance the ice nucleation rate and is not favorable for icephobic characteristics. However, for fluids that show negative slope of solid-liquid phase-change line (e.g. water), the last term is negative (i.e. $(v_w - v_i) < 0$). That is, for these fluids, pressure reduces the ice nucleation temperature and nucleation rate. In other words, the limit of ice nucleation -38 to -40 °C observed in macro-scale is shifted to lower temperatures at nano-scale. T. Li et al.[89] showed the role of nano-scale on suppression of ice nucleation. Through thermodynamic simulation of ice-water system at nano-scale, they demonstrated that Laplace pressure is partially responsible for suppression of ice crystallization. Although this fact is demonstrated in simulations, it remains an open challenge to be demonstrated experimentally.

4. Ice growth

Once ice nucleates, the enthalpy of freezing releases and instantaneously increases the local temperature at the ice-water interface. The heat transfer from the ice-water interface determines the growth rate of ice phase. Let's consider that the freezing front stays at equilibrium temperature (T_f) and neglect the Gibbs-Thompson undercooling effect, Fig. 3 Gibbs-Thompson undercooling effect describes the role of curvature of water-ice interface on temperature of freezing front. Due to this effect, freezing front temperature may be different than that of equilibrium melting temperature. Here, we are studying flat interfaces and this effect can be negligible [90,91]. Note that this assumption does not affect the discussed models below. By including undercooling effect (ΔT), the value of T_f is replaced by $(T_f - \Delta T)$ in below models. We should consider two cases: (I) In an environment with no airflow, Fig. 3a, and (II) In an environment with airflow, Fig. 3b. In case (I) as the air surrounding the droplet has much lower thermal conductivity than ice, the generated enthalpy of phase-change is conducted through the ice and subsequently the solid substrate, (\vec{q}^s) . That is, the heat flux of \vec{q}^l is negligible and the liquid on top of the freezing front stays at isothermal condition. The normal velocity of freezing front, \vec{v}_n , can be represented by the temporal height/radius of the freezing front $(v_n \sim -\frac{dl}{dt} =$ $-\frac{dr}{dt}\frac{(1-\cos\theta)}{\sin\theta}$). The energy balance at the interface for a quasi-steady process is written as $\vec{q} = \rho_i \vec{v}_n H_m$, where ρ_i denotes the density of ice, H_m the enthalpy of ice formation, and \vec{q} the heat transfer away from the interface to the substrate. The value of \vec{q} is written as

$$\vec{q} = \frac{-\delta T}{(\frac{l_0 - l}{k_i} + \frac{l_m}{k_m})}\tag{7}$$

Where $(\delta T = T_s - T_f)$ is the temperature difference between the solid and phase-change

temperature, l_0 is the initial height of the droplet, k_i is the thermal conductivity of ice, l_m is the thickness of substrate and k_m is the thermal conductivity of substrate. Through **Eq. 7** and energy balance at the water-ice interface, one finds

$$\frac{-\delta T}{(\frac{l_0 - l}{k_i} + \frac{l_m}{k_m})} = \rho_i \left(-\frac{dl}{dt}\right) H_m \tag{8}$$

For $l_m/k_m \ll l_0/k_i$ (e.g. high thermal conductivity icephobic material or thin icephobic coatings)

$$l = l_0 - \sqrt{\frac{-2 k_i \delta T}{\rho_i H_m} t}$$

$$\tag{9}$$

And for $l_m/k_m \gg l_0/k_i$ (e.g. low thermal conductivity icephobic material or thick icephobic coatings)

$$l = l_0 + \frac{k_m \,\delta T}{\rho_i \,H_m \,l_m} \,t \tag{10}$$

Note that **Eqs. 9** and **10** may be rewritten in terms of radius of droplet (r) as well. In this analysis, we have adopted quasi-steady heat transfer assumption in which time scale for growth (r/v_n) is larger than the time scale for thermal diffusion (r^2/D_i) , where D_i denotes the thermal diffusivity of ice. For a water droplet with diameter of 1 mm, the time scale for growth is in order of 10 s while the time scale for diffusion is in order of 1 s. This justifies the quasi-steady heat transfer assumption. If one solves the heat equation in the ice domain $(\nabla^2 T = 0)$ with an isothermal boundary condition at the ice-water interface and the prescribed temperature at the ice-solid substrate, one can determine the isotherms in the ice. We extracted reported data on ice growth rate in the literature and conducted some experiments on ice growth on few model surfaces (i.e. PDMS and Glass with thickness of 10 mm) to assess accuracy of the developed model on ice growth rate. The predicted ice growth rate by **Eqs. 9 and 10** are plotted along with

the measured experimental data in **Fig. 4**. As shown, the heat transfer analysis predicts growth rate of ice on various substrate and temperatures with high accuracy. For example, Yao et al.[92] measured freezing time of a water droplet on a stainless-steel surface is measured as 9.6 s and 7 s at temperature of -20 °C and -30 °C, respectively. This predicted freezing time by above models are 6 s and 10 s. Thus, ice accretion rate on a surface could be tuned through manipulation of heat transfer mechanism on the surface. For example, freezing time could be reduced through low thermal conductivity materials or superhydrophobic surfaces (i.e. trapped air on the surfaces).

The above argument holds for a droplet in low convective flow environment. However, in case (II), when the water droplet is exposed to airflow, the convective heat transfer at the surface could reduce the surface temperature and ice nucleation can occur at the liquid-vapor interface as shown by Jung et al.[41]. For this case, **Fig. 3b**, the ice growth rate can be calculated through an energy balance at the phase changing interface. The released enthalpy of freezing is carried away through heat flux at the ice-air interface through convective heat transfer ($\vec{q}_{conv} = \overline{h}_{conv}(T_s - T_{\infty})$), where \overline{h}_{conv} denotes convective heat transfer coefficient. Note that once an ice layer forms on the droplet surface, no further evaporation occurs at the surface. For an external flow over the droplet, the Nusselt number is given by Whitaker[93]

$$\overline{Nu}_D = 2 + \left(0.4 Re_D^{\frac{1}{2}} + 0.06 Re_D^{\frac{2}{3}}\right) Pr^{0.4} \left(\frac{\mu}{\mu_s}\right)^{1/4}$$
(11)

Where $\overline{h}_{conv} = \overline{Nu}_D \frac{\kappa}{D}$, Re_D is Reynolds number, Pr is Prandtl's number (e.g. for air 0.75 at -20 °C), and μ is dynamic viscosity. Thus, having the Reynolds number of an external flow, one can determine the heat transfer coefficient.

As discussed, the energy balance at the water-ice interface for a quasi-steady process is written

as $\vec{q} = \rho_i \vec{v}_n H_m$, where $\vec{v}_n = \frac{-dr_i}{dt}$. Also, in steady-state, $\vec{q} A_i = \vec{q}_{conv} A_o$ and consequently

$$\left(\rho_i \frac{-dr_i}{dt} H_m\right) A_i = \overline{h}_{conv} \left(T_{r=r_o} - T_{\infty}\right) A_o \tag{12}$$

where A denotes surface area. To determine the growth rate of ice layer, $\frac{-dr_i}{dt}$, one needs to determine the surface temperature. We solved heat equation in a spherical coordinate with Robins' boundary condition at the droplet surface $(-k_i \frac{\partial T}{\partial r}\Big|_{r=r_o} = \overline{h}_{conv} \ (T_{r=r_o} - T_{\infty}))$ and prescribed boundary condition at ice-water interface $(T_{r=r_i} = T_f)$. We defined $\theta = T - T_{\infty}$, and $r^* = r_i/r_o$. The solution of heat equation in the ice domain with the given boundary condition is written as (See Appendix C),

$$\frac{\theta_s}{\theta_f} = \frac{r^*}{r^* + Bi(1 - r^*)} \tag{13}$$

Where $Bi = \frac{hr_o}{k}$ and denotes Biot number. Once the **Eq. 13** is replaced in **Eq. 12 and** integrated, the rate of ice layer growth is written as

$$t = \frac{-r_o \rho_i H_m}{6 h \theta_f} (2 (1 - Bi) r^{*3} + 3 Bi r^{*2} - Bi - 2)$$
 (14)

Eq. 14 provides a tool to predict the growth rate of a freezing droplet in high wind condition. We plotted **Eq. 14** for several temperatures and air velocity conditions as shown in **Fig. 5**. The curves suggest that the formation of thin ice layer around the droplet is slow, but further growth of ice layer is fast. We should reiterate that ice nucleation and ice growth are governed by different physics. In the work by Jung et al. [41], on superhydrophobic samples under airflow condition, humidity leads to a transition from nucleation at liquid-vapor interface (homogenous nucleation) to nucleation at solid-liquid interface (heterogenous nucleation). That is, at humidity of 30-75%, ice nucleation occurred at liquid-vapor interface. However, for humidity close to

100%, ice nucleation occurred at solid-liquid interface. This transition is caused by evaporation phenomenon which is governed by humidity gradient. At low humidity, evaporation cooling drops temperature of the liquid-vapor interface and leads to ice nucleation at the liquid-vapor interface. However, at humidity of 100%, evaporation phenomenon is suppressed and ice nucleation occurs at solid-liquid interface. Thus, humidity plays a role in ice nucleation. However, once ice nucleates and a shell forms on the droplet, ice growth is governed by the heat transfer (i.e. convective heat transfer coefficient). The role of humidity in ice growth is hidden in the heat transfer coefficient as humidity could increase thermal conductivity of flowing air. Here, we discussed ice growth for a single isolated droplet. However, for the case of clusters of droplets, ice bridging phenomenon could happen between the droplets. In this case, once a droplet is frozen, the vapor pressure on the ice surface is suppressed and a water vapor gradient occurs between ice and the neighbor supercooled droplets. This vapor gradient leads to formation of ice bridge from the ice to the supercooled water droplet. More discussion on this problem is provided in [29,64].

In summary, we have provided mathematical models for growth rate of ice in two extreme cases (i.e. no flow environment and highly convective flow environment). These analytical models are based on the energy and mass conservations with no fitting parameters. The models could be used to predict freezing of droplets in various environmental conditions. In some cases, the superposition of these two cases may occur. That is, a droplet may freeze initially at the liquid-air interface and forms an ice shell and afterwards the growth front advances from the solid-liquid interface. In these cases, ice growth rate could be calculated through superposition of **Eq. 9 or 10** and **Eq. 14**. An example of this mixed ice growth scenario is shown by Jung et al. [41] in which droplet freezing on a surface under shear flow is examined. A thin ice shell forms on the

droplet in a matter of few milliseconds and afterwards the growth front follows the scheme shown in Fig. 3a.

5. Ice adhesion on a surface

Once ice forms on a surface, the interaction between ice and the substrate will be governed by van der Waal's force, electrostatic forces or hydrogen-bonding forces[94,95]. A wide range of surfaces has been studied to reduce ice adhesion strength. Among those, elastomers have shown the minimum ice adhesion and are of immense interest to reach exceptional icephobic surfaces[22,62]. The remarkable icephobic characteristics of some of these surfaces is caused by non-frozen interfacial water that are discussed below in section 7. Let's consider a rigid ice phase attached to an elastomer as shown in **Fig. 6a**. If the force is applied at a plane higher than the interface, the ice would detach at a critical stress, the force, *F*, applied at a plane slightly above the interface generates an external torque leading to a normal stress at the interface,

$$F. l = a \int \sigma_n x \, dx \tag{15}$$

where a denotes the dimension of ice, σ_n the normal stress at the interface, and x is the horizontal axis. Note that $F = a^2 \sigma_s$, where σ_s is the adhesion stress of the interface (i.e. $\sigma_s \sim \left(\frac{a}{l}\right)\sigma_n$). Note that if a force is applied in the plane of ice-coating, the ice would only slide with no detachment from the surface [96] ($\sigma_s \neq 0$: $l \to 0 \Rightarrow \sigma_n \to 0$). It has been shown by Chaudhury et al.[96] that the elastic instability at the interface of a rigid body and an elastomer is responsible for the detachment. The elastic energy of the elastomer can be simplified by taking into account the equation of continuity and is written as[96]

$$U \sim Gh \,\delta^2 \,\left[\frac{\lambda}{h^2} + \frac{1}{\lambda}\right]^2 \tag{16}$$

where G denotes shear modulus of the elastomer, h is the characteristic length, δ is the amplitude of perturbation of the elastomer film and λ is the wavelength of the elastic waves at the interface. Minimization of this energy with respect to λ results into $\lambda \sim h$. By taking the derivate of the elastic energy with respect to δ , one finds that the normal stress at the interface is $\sigma_n \sim G \delta/h$. The total energy of the elastomer-ice system per unit width (U) is expressed as

$$U = \left(\int_0^a \int_0^{\delta^*} \sigma_n \, d\delta \, dx\right) - W_a a \tag{17}$$

where δ^* denotes the maximum displacement at the interface caused by the instability and W_a is the work of adhesion. The first term represents stored elastic energy in the elastomer and the second term represents the surface energy. The critical stress is found through setting the derivate of total energy with respect to crack length equal to zero. By using the definition of σ_n , one finds,

$$W_a \sim \frac{G\delta^{*2}}{h} \tag{18}$$

For a uniform elastomer with isotropic properties and linear correlation of vertical displacement with respect to a (i.e. $\delta^* \sim a$), one finds that the adhesion stress at the interface is equivalent to

$$\sigma_s \sim \left(\frac{a}{l}\right) \sqrt{\frac{W_a G}{h}}$$
 (19)

This formulation suggests us that low ice adhesion can be achieved through low values of G and W_a . Note that the value of G can be tuned by several orders of magnitude, but the value of W_a in the best case can be tuned by an order of magnitude (e.g. introduction of perfluorinated groups on a surface). By tuning the substrate from hard elastomers ($G \sim 1 \, GPa$) to gel ($G \sim 1 \, kPa$), researchers have been able to reduce ice adhesion[97]. However, low values of G leads to low durability of the icephobic coatings in long-term performance and is not favorable.

We collected some reported values of ice adhesion on various elastomers and plotted the dependence of ice adhesion as a function of $\sqrt{W_aG/h}$ in **Fig. 7**. As shown the reported values agree with the theory within the reported error bars. The values of a, l are determined by the experimental system. Inconsistency in these geometrical parameters for measurement of ice adhesion has resulted in scattered data of ice adhesion for a same substrate [22,98,99] (i.e. PDMS).

In the next section, we have developed a standard approach to measure ice adhesion. This standard approach provides a platform to accurately compare the reported values of ice adhesion by various laboratories.

5.1. Standard procedure for ice adhesion measurement

There are three common methods for ice adhesion measurement. (I) Peak force method [22], Fig. 6a: in this approach, test columns with a pre-defined geometry (e.g. Cuvette) are placed on a cold icephobic substrate. Water is poured into the test columns and consequently ice encase the test column and adhere to the icephobic substrate. The force required to detach each ice column from the icephobic substrate is measured through a force meter. The maximum measured force at break is converted into ice adhesion strength by dividing over cross-sectional area of the ice-substrate interface. (II) Centrifugal force method[100–102], Fig. 6b: in this approach, tip of a wing or a beam is coated with icephobic material. Ice is formed on top of the icephobic material through rain of sub-cooled droplets or through a cuvette ice column. The rotational speed of the beam is gradually increased to induce shear force at the interface of ice-icephobic substrate. At the moment of detachment of ice from the icephobic substrate, the centrifugal force along with cross-sectional area of detached ice provide ice adhesion strength. (III) Tensile force method[51], Fig. 6c: in this method, two concentric aluminum cylinders with a pre-defined gap between

cylinders and a tensile machine test is required. The inner surface of the large cylinder is coated with icephobic material while the outer surface of the small cylinder remains intact. The gap between cylinders is filled with water and the assembly is left in the freezer at a specified temperature for ice formation. Once ice formed between cylinders, the concentric cylinders assembly is placed in the tensile machine and a pulling force is applied to the inner cylinder. As the ice adhesion on aluminum (i.e. outer surface of the small cylinder) is high, ice is detached at the ice-icephobic material interface. At the detachment point, the pulling force divided by the area of ice-icephobic interface gives the value of ice adhesion strength. In all these approaches, the geometry and dimension of the experimental setups affect the measured value of ice adhesion. Work et al. [103] has conducted a thorough review on the approaches for ice adhesion measurements including centrifugal approach, shear stress approach and tensile stress approach and has discussed the source of error in these measurement approaches.

Here, we present a standard procedure for measurement of ice adhesion. The lack of this standard method in the literature has resulted in a wide range of reported ice adhesion values for the same sample. For example, the reported values of ice adhesion for PDMS varies in the range of 100-800 kPa[22,98,99]. Although the discussed physics is focused on elastomers, the standard procedure could be used for various type of icephobic materials.

The adhesion on elastomers depends on the applied shear rate and the geometry of the experimental setup (i.e. a, l, and h). Note that at small shear rates, the ice can slide on the surface for a long distance with no detachment [96]. Thus, it is required to find a shear rate at which the critical shear stress is achieved and fracture occurs at the interface. This critical shear rate depends on the shear modulus of the elastomer. The critical shear rate is an inverse function of shear modulus[96]. Through studies of different elastomers with shear modulus in the range of

0.5 MPa-100 MPa and thickness of 300 \pm 20 μm , we found that the upper limit of critical shear rate for the measurement of ice adhesion is 0.1 mms⁻¹. This shear rate is consistent with the shear rate reported by Meuler et al.[22] In addition to shear rate, we should define the values of geometrical parameters for a standard test. In the derivation of Eq. 19, lubrication approximation of the Stokes equation is used to determine the hydrostatic pressure field in the elastomer. This approximation is valid as long as the a and h satisfy $\frac{a}{h} \gg 1$. Thus, in the standard experimental procedure, we define the value of a as 15 mm and the value h to 300 μ m. We chose 300 μ m as most of the industrial coatings have similar thicknesses. However, any other values that satisfies $\frac{a}{h} \gg 1$ could be used as long as it is documented carefully for comparison purpose. Furthermore, in the derivation of Eq. 19, linear relation between the vertical displacement of the ice and horizontal length scale is considered. This linear relation requires $l/a \ll 1$. Thus, we define the value of l as 3 mm in all the experiments. In summary, the parameters for standard ice adhesion measurement are tabulated in **Table 1**. This standard method provides a rational and unified approach to compare ice adhesion of coatings reported by various laboratories with the same metrics.

6. Durability of icephobic surfaces

Icephobic surfaces are exposed to various conditions including mechanical abrasion and wear, sand or droplet impact, chemical contaminants, ambient temperature variation, and long-time sun exposure. Thus, to ensure long-time performance, icephobic materials should possess mechanical, chemical and environmental durability. The assessment of these durability for icephobic surfaces should be conducted through standard methods with consistent results across various laboratories. There are two standard methods to assess mechanical durability of icephobic coatings: (I) Taber abrasion test according to ASTM D4060[104–108] and (II)

Hardness test according to ASTM D3363[109]. In Taber abrasion test, the icephobic sample is placed firmly on a horizontal platform in the Taber instrument and is exposed to an abrader with various loading conditions (e.g. 1, 5, and 10 N). The fine abrader is CS-10, the medium abrader is H-18 and the hard abrader is CS-17. The number of abrasion cycles varies and it can be few cycles to more than 10000 cycles. The mechanical durability of material in is given by wear index, which is written as

$$Wear index = \frac{B - A}{C} \tag{20}$$

Where *B* denotes weight of specimen after the abrasion test, *A* is the weight of specimen before abrasion test, and *C* is the number of cycles. Note that if during the test, the icephobic coating is completely abraded and the abrader touches the substrates, the results are not reliable and the test should be re-conducted with smaller number of cycles. Once the abrasion test is conducted, the icephobic characteristics of the icephobic surfaces should be re-examined. These tests include ice formation temperature and ice adhesion. For most of the surface-modified approaches (i.e. superhydrophobic surfaces or hydrated-surfaces), failure on icephobicity appears after the abrasion test. As the surface abrades and loses its surface properties, the icephobic characteristics changes. That is, in general, surfaces with volumetric icephobicity show higher long-time performance than surface-modified approaches.

The other test on mechanical durability is film hardness, which is conducted according to pencil test, ASTM D3363[109]. In this standard approach, the icephobic coating is examined by a range of pencils with various hardness from 6B to 6H. Starting through hardest pencil, 6H, the pencil is placed on the coating and is moved over the coating while pushing downward firmly. The procedure is repeated for all the pencils in the order. Gouge hardness is defined as the hardest

pencil that leave the film uncut for a stroke length of at least 3 mm. Scratch hardness is defined as the hardest pencil that will not rupture or scratch the film. In addition to these two methods for assessment of mechanical durability, the developed icephobic material should have a good adhesion to the underlying substrates. The standard method to assess this adhesion is ASTM D3359[110]. In this standard, adhesion of a coating on a substrate is measured through a tape test. Briefly, two cross cutline are made on the coating through a shape blade. The cut should be deep enough to reach to the underlying substrate. A tape is placed and firmly applied to the cross cut to completely cover it. After 90 s, the tape is rapidly peeled from the substrate with the angle of close to 180°. The extent of detachment of icephobic coating is the criterion for assessment of coating adhesion on the substrate.

Depending on the application, icephobic surfaces may be exposed to various chemical environments. For example, the icephobic surfaces in polluted cities could be exposed to acidic rains; the icephobic surfaces on a ship hull are in continuous exposure to salty water; icephobic surfaces on cars could be exposed to salts and cleaning chemicals. Thus, assessment of chemical durability is another essential factor in long-time performance of the icephobic materials.

Durability of a coating to humidity is assessed through ASTM D2247[111]. In this standard procedure, the icephobic coating is exposed to saturated vapor at temperature of 38 °C for a specified duration of time. The extent of color change or blistering of the coating is used as a metric to assess the coating durability. Durability of coatings exposed to corrosive environments is examined through ASTM D1654[112]. In this method a V-shape cut is made on the substrate through a scribing tool. The sample is exposed to a corrosive chemical for a specific time duration. The corrosive chemical should be determined based on the application of the icephobic

coating. After exposure, the coating is cleaned and the extent of the damage to the substrate and coating around the V-shape cut is used as a criterion for chemical durability.

The anticipated life span for an icephobic coating is governed by its resistance to weather conditions. The weathering conditions such as ultraviolet (UV) radiation and humidity have a negative impact on the coatings as they may lead to degradation, yellowness and color change in coatings. Numerous methods have been devised to measure the influence of UV radiation on different polymers. One of these methods is exposure of polymers to natural weather conditions. In this method, samples are placed on an inclined rack that are directed towards the sun with a 45-degree tilt. The 45-degree angle was chosen for full exposure of the solar radiation, which ranges from IR to UV radiation. The disadvantage that comes along with this method is that it takes several years before any significant changes are observed. However, to avoid long waiting periods while testing, accelerated weathering chambers (QUV chambers) are usually used to expedite the testing process. In a standard procedure, ASTM G154[113], a fluorescent UV chamber is used to simulate weather conditions. The test samples are typically flat plaques or disks. The standard sample holders can hold one 3×12 inch (75 \times 300 mm) sample or two 3 \times 6 inch $(75 \times 150 \text{ mm})$ samples. After successfully mounting the samples in the QUV, the samples will be subjected to cycles of exposure to intense ultraviolet radiation followed by moisture exposure by condensation. A typical testing cycle is to expose the coating to 8 hours of UV exposure (irradiance of 0.49 W/m².nm at 310 nm wavelength) at 70 °C followed by 4 hours of condensation at 50 °C. These cycles are repeated for 2000 hours. At the end of this exposure, the properties of the icephobic coating including visual and integrity of the coating, mechanical durability, chemical durability and ice adhesion strength is examined. We should add icephobic properties of some coatings depends on icing/de-icing cycle [102,114]. For long-term durability

assessment, these surfaces should go through icing/de-icing process and icephobic figures of merit be examined after each cycle. We have summarized these standard durability tests in **Table** 2.

7. State-of-the-Art Icephobic Surfaces

Below, we present state-of-the-art icephobic surfaces and discuss their characteristics through the discussed metrics above. These surfaces are shown schematically in Fig. 8. Superhydrophobic surfaces (SHS), Fig. 8a, are developed through micro/nano structuring on hydrophobic surfaces[115-119] (or hydrophilic surfaces[120,121]). These surfaces trap air and prevent wetting (Cassie-Baxter state) to minimize the effective contact area between stationary or dynamic subcooled droplets and the cold solid substrate[18-60]. The hydrophobic nature of these surfaces affects the thermodynamics of ice nucleation [41,73,75,77,122–125] through m parameter in f(m, x) and the reduction of solid-ice contact area can affect the heat transfer in ice growth (i.e. ice accretion rate) and the mechanics of solid-ice interface (i.e. ice adhesion strength)[58,76]. As discussed, from a thermodynamic perspective, T_N is a function of interfacial energy of solid-water combination and dimension of micro/nano features through Gibbs energy barrier [78,126]. For a given solid, Gibbs energy barrier is not affected unless micro/nano features are dimensionally in the same order of ice embryo (few nms)[78]. Surfaces with such small features are difficult and expensive to fabricate. Thus, for most studied superhydrophobic surfaces, the median ice nucleation temperature is in the range of -20 till -25 °C[77]. By contrast, the homogeneous ice nucleation temperature of bulk water is -40 °C [127,128], which provides a lower practical limit and target for designing icephobic surfaces where nucleation occurs heterogeneously. As discussed in Eq. 4, τ_{av} is also a function of Gibbs energy barrier. At a given temperature, ice nucleation delay time therefore remains unaffected unless the heterogeneous

energy barrier is tuned. Although the droplet contact area on superhydrophobic surfaces may be reduced, the molecular nature of solid-ice interaction (i.e. W_a) and the mechanical properties of the icephobic surfaces affects ice adhesion strength. The reported ice adhesion on superhydrophobic surfaces is in the order of 100-500 kPa, which is of similar magnitude to adhesion strengths measured on smooth metal surfaces (~100 kPa)[22,59,129–136]. Once frost forms between micro/nano structures on SHS, water droplet sitting on the surface transforms to Wenzel state and fill the micro/nano features of the structure. In this case, ice adhesion can become even higher than smooth surface. Despite extensive studies on icephobicity of SHS so far, low ice adhesion along with mechanical durability on SHS has not yet been achieved. In a promising approach, Sojoudi et al. [137,138] developed hydrophobic surfaces through grafting of Poly-(1H,1H,2H,2H-perfluorodecylacrylate) (pPFDA) by iCVD method on smooth metals. These surfaces are mechanically durable and reduce ice adhesion on metals by an order of magnitude.

Recently, new icephobic surfaces called slippery liquid infused porous surfaces (SLIPS), **Fig. 8b**, have been created, which utilize the smooth nature of liquid surface to improve icephobicity[20,61]. These surfaces were inspired by the Nepenthes pitcher plant[139]. SLIPS are developed by entrapping a liquid in a porous media through capillary forces. Despite formation of thin liquid film, the value of T_N and τ_{av} are similar to the superhydrophobic surfaces at \sim -25 $^{\circ}$ C[140]. The smooth nature of liquid surface mitigates pinning of water droplets on these surfaces[141] and reduce ice adhesion strength[142–155] to values of 10-150 kPa. However, after few cycles of icing-deicing, the liquid layer is depleted and the ice adhesion increases to the order of 200 kPa. This behavior is discussed in Irajizad et al. [81] and several other studies[153,156–158]. For example, Rykaczewski et al.[65], who studied freezing of sub-

cooled condensate on SLIPS, found that water droplets infuse into the bulk of the oil where they form an interface with the solid and deplete oil film as they move on the surface.

One of the interesting feature of ice is the existence of a thin liquid-like transition layer at the surface even at freezing temperatures, which makes ice slippery[159–163]. This thin film makes it possible to skate at freezing temperatures. This feature has been exploited in development of hydrated icephobic surfaces, **Fig. 8c**, that promote formation of aqueous lubricating layer with no need for additional oil. While the lubricating film exist on the surface (i.e. in the temperature range of 0 to -25 °C), ice adhesion on these surfaces is in the range of 20-60 kPa[27,131,133,164]. However, at lower temperatures, the change in molecular configuration of the transition film drastically boosts the ice adhesion to values in the order of 1000 kPa[27]. The idea of a non-frozon liquid-like layer at the ice surface inspired Chen et al.[62] to develop a new type of icephobic surfaces that keeps a quasi-liquid layer on its surface. These surfaces were developed through blending of polydimethylsiloxane (PDMS)-poly(ethylene glycol) (PEG) amphiphilic copolymers into a polymer matrix and show ice adhesion strength of 50 kPa.

In another thoughtful approach, Golovin et al.[165] exploited modified elastomers to reduce ice adhesion. In this approach, the shear modulus of various elastomer was tuned by reducing the cross-linking density of the structure and interfacial slippage was activated at the interface through embedding miscible polymeric chains. The authors reported that the stress required for motion of ice on the surface is in the range of 0.2-10 kPa. However, the stress required for motion of ice on a surface is different than the adhesion stress. While in the former case, ice is still in contact with the surface, in the latter one the induced stress detach ice from the surface. The adhesion stress is the critical stress (maximum stress) that ice detaches from the surface. Furthermore, the adhesion stress on elastomers is a function of shear rate and can vary by an

order of magnitude depending on the applied shear rate. Thus, to compare these values of ice adhesion with the other reported values, a standard test protocol needs to be followed. Even recently, Vasileiou et al.[166] showed that flexibility of the substrates could lead to reduce adhesion of ice on a substrate.

In a recent approach, Irajizad et al. [167] developed concept of stress-localization to reduce adhesion of ice on a surface, **Fig. 8d**. In this approach, a low shear modulus material, phase II, is dispersed in a high shear modulus matrix, phase I. Once ice forms on these surfaces, with a minimal force, ice is detached from phase II and forms cavities at the interface of ice and the icephobic material. A stress field at the perimeter of cavity is then induced leading to growth of crack/cavity at the interface and fracture. In contrast to other surface-modification approaches (e.g. superhydrophobic, slips and hydrated surfaces), stress-localization effect is a volumetric phenomenon and remains effective even after long-time operation of these surfaces. Ice adhesion on these surfaces is in order of 1-10 kPa while having high mechanical, chemical and environmental durability.

We summarized ice adhesion on all reported icephobic surfaces in **Fig. 9**. These include smooth polymers, ceramics and metals to micro/nano structured surfaces and recent advanced surfaces. Variation in the reported ice adhesion for a surface comes from inconsistency in the measurement's approaches. This graph demonstrates importance of a standard method for ice adhesion assessment. Otherwise, comparison of icephobic performance of different surfaces is not possible. Durable icephobic surfaces with ice adhesion smaller than 10 kPa is in high demand in various fields. Furthermore, we have listed measured ice adhesion on various icephobic surfaces in **Table 3** along with method of measurements. For most of the surfaces, the measurement method is cuvette-encased ice columns. However, even in this method, the

thickness of sample and geometrical parameters (a, l) affect measured ice adhesion and a standard protocol needs to be followed.

In summary, there is a high demand to explore new material systems along with rational geometrical structuring to develop durable icephobic surfaces. Any proposed icephobic material should be thoroughly examined with all the discussed figures of merit to assure their superior properties. The standard methods elaborated above provide a platform to compare the reports from various laboratories and guide the scientific community in an optimized approach to find new icephobic materials.

8. Conclusion and outlook

A comprehensive definition of icephobic surfaces is provided which includes low ice formation temperature, low ice accretion rate, low ice adhesion strength and mechanical, chemical and environmental durability. The ice formation temperature is governed by thermodynamics, ice accretion rate is governed by heat transfer, ice adhesion strength is governed by mechanics of solid-ice interface and durability is governed by the material properties. All these physics are thoroughly discussed and several predictive models are developed and validated by the reported data in the literature. Furthermore, the role of length scale in these physics is highlighted. This fundamental physics provides a rational pathway to achieve superior icephobic material.

Based on this definition of icephobicity, a set of standard figures of merit is developed for unbiased assessment of icephobic surfaces. Absence of these standard figures of merit has resulted in orders of magnitude discrepancy between reported results for the same icephobic surface by various laboratories. Through the developed comprehensive framework, performance of state-of-the-art icephobic surfaces are compared. The comparison suggests that further research is required to achieve low ice adhesion along with high durability. Furthermore, ice

nucleation temperature and ice accretion rate are important metrics which have been overlooked

so far. Physics-based and rational approaches are in demand to address these metrics.

AUTHOR INFORMATION

Corresponding Author

*E-mail: hghasemi@uh.edu

ACKNOWLEDGMENT

The authors gratefully acknowledge funding support from National Science Foundation (Grant

NSF- 1804204) with Dr. Susan Muller as program manager and Air Force Office of Scientific

Research (Grant AFOSR FA9550-16-1-0248) with Dr. Ali Sayir as program manager.

Appendices

Appendix A: Ice nucleation temperature and average nucleation delay time

Ice nucleation temperature (T_N) : is defined as the nucleation temperature of a sessile water

droplet placed on a surface when the system of droplet, surface and surrounding is cooled in a

quasi-equilibrium approach [77].

T_N measurement approach: The icephobic sample is placed in a nitrogen chamber with initial

temperature of 0 °C. A droplet of distilled water (volume of 30 µL) is introduced on the sample's

surface at this temperature. The chamber is cooled with cooling rate of 1°C/10 min. Several

thermocouples are installed to probe temperature of the sample and the surrounding environment

to ensure isothermal condition. Two thermocouples are attached to the sample with a thermal

paste. Temperature of the sample is recorded as close as possible to the droplet without causing

disturbance to the experiment. The droplet is visualized with a camera during this cooling

29

process. Once ice nucleates, suddenly the droplet transparency changes and the sample temperature is recorded. This process is repeated for > 10 times and the average nucleation temperature is considered T_N [77,81].

Average nucleation delay time (τ_{av}): is defined as the average time required for ice nucleation of a supercooled droplet in thermal equilibrium with its surrounding [77].

 τ_{av} measurement approach: The icephobic sample is placed in an isothermal chamber. Temperature of the chamber and the sample are adjusted to a subzero temperature. A water droplet is placed on the sample. The time required for ice nucleation at the given temperature is captured through high-speed imaging of the droplet. Similar to T_N experiment, one should repeat these experiments for > 10 time and report the median time as τ_{av} [77,81].

Appendix B: Critical Nucleolus radius

The critical ice nucleolus radius [78,126] is

$$\mathbf{r}_{\mathbf{c}} = \frac{2\gamma_{IW}}{\Delta G_{f,v}}$$

Where $\Delta G_{f,v}$ and γ_{IW} are written as $\Delta G_{f,v} = \Delta H_{f,v} \frac{(T_m - T)}{T_m}$ and $\gamma^{IW} = 23.24 (\frac{T}{235.8})^{0.35}$.

Appendix C: Ice growth rate in a highly convective environment

Through solution of heat equation in a spherical coordinate, one finds

$$\frac{1}{r^2}\frac{\partial}{\partial r}\left(r^2\frac{\partial T}{\partial r}\right) = 0 \implies r^2\frac{\partial T}{\partial r} = C_1 \implies \frac{\partial T}{\partial r} = \frac{C_1}{r} \tag{1}$$

And

$$T = -\frac{C_1}{r} + C_2 (2)$$

Temperature at ice-water and ice-air interface is given as $T(r = r_i) = T_f$ and $T(r = r_0) = T_s$, respectively. The boundary conditions are written as

@
$$r = r_i$$
: $T = T_f$

Through applying boundary condition on Eq. 2, one finds,

$$T_{f} = -\frac{C_{1}}{r_{i}} + C_{2}$$

$$h\left(-\frac{C_{1}}{r_{0}} + C_{2} - T_{\infty}\right) = -k_{i}\left(\frac{C_{1}}{r_{0}^{2}}\right)$$

$$C_{1} = (T_{\infty} - T_{f})\left(\frac{k_{i}}{hr_{0}^{2}} - \frac{1}{r_{0}} + \frac{1}{r_{i}}\right)^{-1}$$

$$C_{2} = T_{\infty} - \frac{k_{i}}{h}\left(\frac{C_{1}}{r_{0}^{2}}\right) + \frac{C_{1}}{r_{0}}$$

We define,

$$\theta_f = T_f - T_{\infty}$$

Thus,

$$C_1 = -\theta_f \left(\frac{k_i}{hr_0^2} - \frac{1}{r_0} + \frac{1}{r_i} \right)^{-1} \tag{3}$$

And

$$C_2 = T_{\infty} + \theta_f \left[1 - \left(\frac{k_i r_i}{h r_0^2} - \frac{r_i}{r_0} + 1 \right)^{-1} \right]$$
 (4)

The surface temperature is written as

$$T_s = -\frac{C_1}{r_0} + C_2$$

We define $r^* = \frac{r_i}{r_0}$ and $\theta_s = T_s - T_\infty$. By substation of C_1 and C_2 , one finds the following function for θ_s

$$\theta_s = \frac{\theta_f}{r_0 \left(\frac{k_i}{hr_0^2} - \frac{1}{r_0} + \frac{1}{r_i}\right)} + \theta_f \left[1 - \left(\frac{k_i r^*}{hr_0} - r^* + 1\right)^{-1}\right]$$

By simplification of this equation, $\frac{\theta_s}{\theta_f}$ is written as

$$\frac{\theta_s}{\theta_f} = \frac{k_i r^*}{k_i (r^* - \frac{hr_0}{k_i} r^* + \frac{hr_0}{k_i})}$$

Biot number is defined as

$$B_i = \frac{hr_0}{k_i}$$

And $\frac{\theta_s}{\theta_f}$ may be simplified to

$$\frac{\theta_s}{\theta_f} = \frac{r^*}{r^* + B_i(1 - r^*)} \tag{5}$$

The energy balance at the ice-water interface requires

$$\vec{q} = hA_0(T_s - T_\infty) = \rho_i H_m A_i \left(-\frac{dr_i}{dt}\right)$$

$$h\theta_s = \rho_i H_m \left(-\frac{dr_i}{dt}\right) r^{*2}$$
(6)

By substation of θ_s from **Eq. 5**,

$$h\theta_f(\frac{r^*}{r^* + B_i(1 - r^*)}) = \rho_i H_m(-r_0 \frac{dr^*}{dt})r^{*2}$$

And by simplification of this equation, one finds

$$-\frac{h\theta_f}{r_0\rho_i H_m}(dt) = (r^* + B_i(1 - r^*))r^* dr^*$$

We integrate both sides

$$\int -\frac{h\theta_f}{r_0\rho_i H_m} dt = \int (r^* + B_i(1 - r^*))r^* dr^*$$

$$= > -\frac{h\theta_f}{r_0\rho_i H_m} t = \frac{r^{*3}}{3} + B_i \left(\frac{r^{*2}}{2} - \frac{r^{*3}}{3}\right) + C$$

The initial condition for ice growth is given as

$$t(r^* = 1) = 0$$

and through applying this initial condition, one finds

$$t = -\frac{r_0 \rho_i H_m}{6h \theta_f} (2(1 - B_i)r^{*3} + 3B_i r^{*2} - B_i - 2)$$
(7)

REFERENCES

- [1] Jia Z, DeLuca CI, Chao H, Davies PL. Structural basis for the binding of a globular antifreeze protein to ice. Nature 1996;384:285–8. doi:10.1038/384285a0.
- [2] Liou YC, Tocilj a, Davies PL, Jia Z. Mimicry of ice structure by surface hydroxyls and water of a beta-helix antifreeze protein. Nature 2000;406:322–4. doi:10.1038/35018604.

- [3] Dalili N, Edrisy A, Carriveau R. A review of surface engineering issues critical to wind turbine performance. Renew Sustain Energy Rev 2009;13:428–38. doi:10.1016/j.rser.2007.11.009.
- [4] Andersson AK, Chapman L. The impact of climate change on winter road maintenance and traffic accidents in West Midlands, UK. Accid Anal Prev 2011;43:284–9. doi:10.1016/j.aap.2010.08.025.
- [5] Gent RW, Dart NP, Cansdale JT. Aircraft Icing. Phil Trans R Soc Lond 2000;358:2873–911. doi:10.1098/rsta.2000.0689.
- [6] Marwitz J, Politovich M, Bernstein B, Ralph F, Neiman P, Ashenden R, et al. Meteorological Conditions Associated with the ATR72 Aircraft Accident near Roselawn, Indiana, on 31 October 1994. Bull Am Meteorol Soc 1997;78:41–52. doi:10.1175/1520-0477.
- [7] Laforte JL, Allaire M a., Laflamme J. State-of-the-art on power line de-icing. Atmos Res 1998;46:143–58. doi:10.1016/S0169-8095(97)00057-4.
- [8] Arctic Council. Arctic Marine Infrastructure. 2009.
- [9] Jiang X, Zhao J, Luo B, Zhang J, Huang C. Survey and Analysis of Ice Accidents of Early 2008 in Southern China. IWAIS XIII, Andermatt, Switzerland: 2009.
- [10] Antonini C, Innocenti M, Horn T, Marengo M, Amirfazli A. Understanding the effect of superhydrophobic coatings on energy reduction in anti-icing systems. Cold Reg Sci Technol 2011;67:58–67. doi:10.1016/j.coldregions.2011.02.006.
- [11] Machielsen CHM, Kerschbaumer HG. Influence of frost formation and defrosting on the performance of air coolers: standards and dimensionless coefficients for the system designer. Int J Refrig 1989;12:283–90. doi:10.1016/0140-7007(89)90095-9.
- [12] Mohseni M, Amirfazli A. A novel electro-thermal anti-icing system for fiber-reinforced polymer composite airfoils. Cold Reg Sci Technol 2013;87:47–58. doi:10.1016/j.coldregions.2012.12.003.
- [13] Acharya P V., Bahadur V. Fundamental interfacial mechanisms underlying electrofreezing. Adv Colloid Interface Sci 2018;251:26–43. doi:10.1016/j.cis.2017.12.003.
- [14] Homola MC, Nicklasson PJ, Sundsbø PA. Ice sensors for wind turbines. Cold Reg Sci Technol 2006;46:125–31. doi:10.1016/j.coldregions.2006.06.005.
- [15] Campbell RJ. Weather-Related Power Outages and Electric System Resiliency. Congr Res Serv Rep 2012:1–15. doi:R42696.
- [16] LaCommare KH, Eto JH. Cost of Power Interruptions to Electricity Consumers in the United States (U.S.). 2006.
- [17] Research and Markets. Ice Protection Systems Market Global Forecasts to 2021. 2017.
- [18] Maitra T, Tiwari MK, Antonini C, Schoch P, Jung S, Eberle P, et al. On the nanoengineering of superhydrophobic and impalement resistant surface textures below the freezing temperature. Nano Lett 2014;14:172–82. doi:10.1021/nl4037092.
- [19] Mishchenko L, Hatton B, Bahadur V, Taylor JA, Krupenkin T, Aizenberg J. Design of ice-free nanostructured surfaces based on repulsion of impacting water droplets. ACS Nano 2010;4:7699–707. doi:10.1021/nn102557p.
- [20] Wong T-S, Kang SH, Tang SKY, Smythe EJ, Hatton BD, Grinthal A, et al. Bioinspired self-repairing slippery surfaces with pressure-stable omniphobicity. Nature 2011;477:443–7. doi:10.1038/nature10447.
- [21] Meuler AJ, McKinley GH, Cohen RE. Exploiting topographical texture to impart icephobicity. ACS Nano 2010;4:7048–52. doi:10.1021/nn103214q.

- [22] Meuler AJ, Smith JD, Varanasi KK, Mabry JM, McKinley GH, Cohen RE. Relationships between water wettability and ice adhesion. ACS Appl Mater Interfaces 2010;2:3100–10. doi:10.1021/am1006035.
- [23] Alizadeh A, Bahadur V, Zhong S, Shang W, Li R, Ruud J, et al. Temperature dependent droplet impact dynamics on flat and textured surfaces. Appl Phys Lett 2012;100. doi:10.1063/1.3692598.
- [24] Alizadeh A, Yamada M, Li R, Shang W, Otta S, Zhong S, et al. Dynamics of ice nucleation on water repellent surfaces. Langmuir 2012;28:3180–6. doi:10.1021/la2045256.
- [25] Guo P, Zheng Y, Wen M, Song C, Lin Y, Jiang L. Icephobic/anti-icing properties of micro/nanostructured surfaces. Adv Mater 2012;24:2642–8. doi:10.1002/adma.201104412.
- [26] He M, Wang J, Li H, Song Y. Super-hydrophobic surfaces to condensed micro-droplets at temperatures below the freezing point retard ice/frost formation. Soft Matter 2011;7:3993. doi:10.1039/c0sm01504k.
- [27] Chen J, Dou R, Cui D, Zhang Q, Zhang Y, Xu F, et al. Robust prototypical anti-icing coatings with a self-lubricating liquid water layer between ice and substrate. ACS Appl Mater Interfaces 2013;5:4026–30. doi:10.1021/am401004t.
- [28] Petit J, Bonaccurso E. General frost growth mechanism on solid substrates with different stiffness. Langmuir 2014;30:1160–8. doi:10.1021/la404084m.
- [29] Chen X, Ma R, Zhou H, Zhou X, Che L, Yao S, et al. Activating the microscale edge effect in a hierarchical surface for frosting suppression and defrosting promotion. Sci Rep 2013;3:2515. doi:10.1038/srep02515.
- [30] Boinovich L, Emelyanenko AM, Korolev V V., Pashinin AS. Effect of wettability on sessile drop freezing: When superhydrophobicity stimulates an extreme freezing delay. Langmuir 2014;30:1659–68. doi:10.1021/la403796g.
- [31] Boinovich L, Emelyanenko AM. Role of water vapor desublimation in the adhesion of an iced droplet to a superhydrophobic surface. Langmuir 2014;30:12596–601. doi:10.1021/la503447f.
- [32] Boreyko JB, Collier CP. Delayed frost growth on jumping-drop superhydrophobic surfaces. ACS Nano 2013;7:1618–27. doi:10.1021/nn3055048.
- [33] Oberli L, Caruso D, Hall C, Fabretto M, Murphy PJ, Evans D. Condensation and freezing of droplets on superhydrophobic surfaces. Adv Colloid Interface Sci 2014;210:47–57. doi:10.1016/j.cis.2013.10.018.
- [34] Wang S, Yang Z, Gong G, Wang J, Wu J, Yang S, et al. Icephobicity of Penguins Spheniscus Humboldti and an Artificial Replica of Penguin Feather with Air-Infused Hierarchical Rough Structures. J Phys Chem C 2016;120:15923–9. doi:10.1021/acs.jpcc.5b12298.
- [35] Ruan M, Li W, Wang B, Deng B, Ma F, Yu Z. Preparation and anti-icing behavior of superhydrophobic surfaces on aluminum alloy substrates. Langmuir 2013;29:8482–91. doi:10.1021/la400979d.
- [36] Wang Y, Xue J, Wang Q, Chen Q, Ding J. Verification of icephobic/anti-icing properties of a superhydrophobic surface. ACS Appl Mater Interfaces 2013;5:3370–81. doi:10.1021/am400429q.
- [37] Bahadur V, Mishchenko L, Hatton B, Taylor JA, Aizenberg J, Krupenkin T. Predictive Model for Ice Formation on Superhydrophobic Surfaces. Langmuir 2011;27:14143–50.

- doi:Doi 10.1021/La200816f.
- [38] Sarshar MA, Swarctz C, Hunter S, Simpson J, Choi CH. Effects of contact angle hysteresis on ice adhesion and growth on superhydrophobic surfaces under dynamic flow conditions. Colloid Polym Sci 2013;291:427–35. doi:10.1007/s00396-012-2753-4.
- [39] Maitra T, Antonini C, Tiwari MK, Mularczyk A, Imeri Z, Schoch P, et al. Supercooled water drops impacting superhydrophobic textures. Langmuir 2014;30:10855–61. doi:10.1021/la502675a.
- [40] Hao Q, Pang Y, Zhao Y, Zhang J, Feng J, Yao S. Mechanism of delayed frost growth on superhydrophobic surfaces with jumping condensates: More than interdrop freezing. Langmuir 2014;30:15416–22. doi:10.1021/la504166x.
- [41] Jung S, Tiwari MK, Doan NV, Poulikakos D. Mechanism of supercooled droplet freezing on surfaces. Nat Commun 2012;3:615. doi:10.1038/ncomms1630.
- [42] Zhang Y, Yu X, Wu H, Wu J. Facile fabrication of superhydrophobic nanostructures on aluminum foils with controlled-condensation and delayed-icing effects. Appl Surf Sci 2012;258:8253–7. doi:10.1016/j.apsusc.2012.05.032.
- [43] Wen M, Wang L, Zhang M, Jiang L, Zheng Y. Antifogging and icing-delay properties of composite micro- and nanostructured surfaces. ACS Appl Mater Interfaces 2014;6:3963–8. doi:10.1021/am405232e.
- [44] Boreyko JB, Srijanto BR, Nguyen TD, Vega C, Fuentes-Cabrera M, Collier CP. Dynamic defrosting on nanostructured superhydrophobic surfaces. Langmuir 2013;29:9516–24. doi:10.1021/la401282c.
- [45] Farhadi S, Farzaneh M, Kulinich SA. Anti-icing performance of superhydrophobic surfaces. Appl Surf Sci 2011;257:6264–9. doi:10.1016/j.apsusc.2011.02.057.
- [46] Wang N, Xiong D, Deng Y, Shi Y, Wang K. Mechanically robust superhydrophobic steel surface with anti-icing, UV-durability, and corrosion resistance properties. ACS Appl Mater Interfaces 2015;7:6260–72. doi:10.1021/acsami.5b00558.
- [47] Ge L, Ding G, Wang H, Yao J, Cheng P, Wang Y. Anti-icing property of superhydrophobic octadecyltrichlorosilane film and its ice adhesion strength. J Nanomater 2013;2013. doi:10.1155/2013/278936.
- [48] Kulinich SA, Farzaneh M. How wetting hysteresis influences ice adhesion strength on superhydrophobic surfaces. Langmuir 2009;25:8854–6. doi:10.1021/la901439c.
- [49] Momen G, Jafari R, Farzaneh M. Ice repellency behaviour of superhydrophobic surfaces: Effects of atmospheric icing conditions and surface roughness. Appl Surf Sci 2015;349:211–8. doi:10.1016/j.apsusc.2015.04.180.
- [50] Davis A, Yeong YH, Steele A, Bayer IS, Loth E. Superhydrophobic nanocomposite surface topography and ice adhesion. ACS Appl Mater Interfaces 2014;6:9272–9. doi:10.1021/am501640h.
- [51] Yang S, Xia Q, Zhu L, Xue J, Wang Q, Chen QM. Research on the icephobic properties of fluoropolymer-based materials. Appl Surf Sci 2011;257:4956–62. doi:10.1016/j.apsusc.2011.01.003.
- [52] Tourkine P, Merrer M Le, Quéré D. Delayed freezing on water repellent materials. Langmuir 2009;25:7214–6. doi:10.1021/la900929u.
- [53] Mangini D, Antonini C, Marengo M, Amirfazli A. Runback ice formation mechanism on hydrophilic and superhydrophobic surfaces. Cold Reg Sci Technol 2015;109:53–60. doi:10.1016/j.coldregions.2014.09.012.
- [54] Mandal DK, Criscione A, Tropea C, Amirfazli A. Shedding of Water Drops from a

- Surface under Icing Conditions. Langmuir 2015;31:9340–7. doi:10.1021/acs.langmuir.5b02131.
- [55] Graeber G, Schutzius TM, Eghlidi H, Poulikakos D. Spontaneous self-dislodging of freezing water droplets and the role of wettability. Proc Natl Acad Sci 2017;114:11040–5. doi:10.1073/pnas.1705952114.
- [56] Varanasi KK, Deng T, Smith JD, Hsu M, Bhate N. Frost formation and ice adhesion on superhydrophobic surfaces. Appl Phys Lett 2010;97:23–6. doi:10.1063/1.3524513.
- [57] Kulinich SA, Farhadi S, Nose K, Du XW. Superhydrophobic surfaces: Are they really icerepellent? Langmuir 2011;27:25–9. doi:10.1021/la104277q.
- [58] Sojoudi H, Wang M, Boscher ND, McKinley GH, Gleason KK. Durable and scalable icephobic surfaces: similarities and distinctions from superhydrophobic surfaces. Soft Matter 2016;12:1938–63. doi:10.1039/C5SM02295A.
- [59] Hejazi V, Sobolev K, Nosonovsky M. From superhydrophobicity to icephobicity: forces and interaction analysis. Sci Rep 2013;3:2194. doi:10.1038/srep02194.
- [60] Guo P, Zheng Y, Liu C, Ju J, Jiang L. Directional shedding-off of water on natural/bio-mimetic taper-ratchet array surfaces. Soft Matter 2012;8:1770. doi:10.1039/c1sm06631e.
- [61] Lafuma A, Quéré D. Slippery pre-suffused surfaces. EPL (Europhysics Lett 2011;96:56001. doi:10.1209/0295-5075/96/56001.
- [62] Chen D, Gelenter MD, Hong M, Cohen RE, McKinley GH. Icephobic surfaces induced by interfacial nonfrozen water. ACS Appl Mater Interfaces 2017;9:4202–14. doi:10.1021/acsami.6b13773.
- [63] Sun X, Damle VG, Uppal A, Linder R, Chandrashekar S, Mohan AR, et al. Inhibition of Condensation Frosting by Arrays of Hygroscopic Antifreeze Drops. Langmuir 2015;31:13743–52. doi:10.1021/acs.langmuir.5b03869.
- [64] Nath S, Boreyko JB. On Localized Vapor Pressure Gradients Governing Condensation and Frost Phenomena. Langmuir 2016;32:8350–65. doi:10.1021/acs.langmuir.6b01488.
- [65] Rykaczewski K, Anand S, Subramanyam SB, Varanasi KK. Mechanism of frost formation on lubricant-impregnated surfaces. Langmuir 2013;29:5230–8. doi:10.1021/la400801s.
- [66] Walker C, Lerch S, Reininger M, Eghlidi H, Milionis A, Schutzius TM, et al. Desublimation Frosting on Nanoengineered Surfaces. ACS Nano 2018;12:8288–96. doi:10.1021/acsnano.8b03554.
- [67] Sun X, Rykaczewski K. Suppression of Frost Nucleation Achieved Using the Nanoengineered Integral Humidity Sink Effect. ACS Nano 2017;11:906–17. doi:10.1021/acsnano.6b07505.
- [68] Ahmadi SF, Nath S, Iliff GJ, Srijanto BR, Collier CP, Yue P, et al. Passive Antifrosting Surfaces Using Microscopic Ice Patterns. ACS Appl Mater Interfaces 2018;10:32874–84. doi:10.1021/acsami.8b11285.
- [69] Guadarrama-Cetina J, Mongruel A, González-Viñas W, Beysens D. Frost formation with salt. Epl 2015;110. doi:10.1209/0295-5075/110/56002.
- [70] Piucco RO, Hermes CJL, Melo C, Barbosa JR. A study of frost nucleation on flat surfaces. Exp Therm Fluid Sci 2008;32:1710–5. doi:10.1016/j.expthermflusci.2008.06.004.
- [71] Na B, Webb RL. A fundamental understanding of factors affecting frost nucleation. Int J Heat Mass Transf 2003;46:3797–808. doi:10.1016/S0017-9310(03)00194-7.
- [72] He Z, Xiao S, Gao H, He J, Zhang Z. Multiscale crack initiator promoted super-low ice adhesion surfaces. Soft Matter 2017;13:6562–8. doi:10.1039/c7sm01511a.
- [73] Cao L, Jones AK, Sikka VK, Wu J, Gao D. Anti-Icing superhydrophobic coatings.

- Langmuir 2009;25:12444-8. doi:10.1021/la902882b.
- [74] Zheng L, Li Z, Bourdo S, Khedir KR, Asar MP, Ryerson CC, et al. Exceptional superhydrophobicity and low velocity impact icephobicity of acetone-functionalized carbon nanotube films. Langmuir 2011;27:9936–43. doi:10.1021/la201548k.
- [75] Jung S, Dorrestijn M, Raps D, Das A, Megaridis CM, Poulikakos D. Are superhydrophobic surfaces best for icephobicity? Langmuir 2011;27:3059–66. doi:10.1021/la104762g.
- [76] Nosonovsky M, Hejazi V. Why superhydrophobic surfaces are not always icephobic. ACS Nano 2012;6:8488–91. doi:10.1021/nn302138r.
- [77] Eberle P, Tiwari MK, Maitra T, Poulikakos D. Rational nanostructuring of surfaces for extraordinary icephobicity. Nanoscale 2014;6:4874–81. doi:10.1039/c3nr06644d.
- [78] Fletcher NH. Size Effect in Heterogeneous Nucleation. J Chem Phys 1958;29:572. doi:10.1063/1.1744540.
- [79] Li C, Tao R, Luo S, Gao X, Zhang K, Li Z. Enhancing and Impeding Heterogeneous Ice Nucleation through Nanogrooves. J Phys Chem C 2018:acs.jpcc.8b07779. doi:10.1021/acs.jpcc.8b07779.
- [80] Fox HW, Zisman WA. The spreading of liquids on low-energy surfaces. III. Hydrocarbon surfaces. J Colloid Sci 1952;7:428–42. doi:10.1016/0095-8522(52)90008-1.
- [81] Irajizad P, Hasnain M, Farokhnia N, Sajadi SM, Ghasemi H. Magnetic slippery extreme icephobic surfaces. Nat Commun 2016;7:13395. doi:10.1038/ncomms13395.
- [82] Irajizad P, Ray S, Farokhnia N, Hasnain M, Baldelli S, Ghasemi H. Remote Droplet Manipulation on Self-Healing Thermally Activated Magnetic Slippery Surfaces. Adv Mater Interfaces 2017;4:1700009. doi:10.1002/admi.201700009.
- [83] Masoudi A, Irajizad P, Farokhnia N, Kashyap V, Ghasemi H. Antiscaling Magnetic Slippery Surfaces. ACS Appl Mater Interfaces 2017;9. doi:10.1021/acsami.7b05564.
- [84] Russell KC. Nucleation in solids: the Induction and steady-state effects. Adv Colloid Interface Sci 1980;13:205–318. doi:10.1016/0001-8686(80)80003-0.
- [85] Mullin JW. Crystallization. 4th ed. Woburn: Reed educational and professional publishing; 2001.
- [86] Liu H, Cao G. Effectiveness of the Young-Laplace equation at nanoscale. Sci Rep 2016;6:1–10. doi:10.1038/srep23936.
- [87] Walther JH, Ritos K, Cruz-Chu ER, Megaridis CM, Koumoutsakos P. Barriers to superfast water transport in carbon nanotube membranes. Nano Lett 2013;13:1910–4. doi:10.1021/nl304000k.
- [88] Cottin-Bizonne C, Barentin C, Charlaix É, Bocquet L, Barrat JL. Dynamics of simple liquids at heterogeneous surfaces: Molecular-dynamics simulations and hydrodynamic description. Eur Phys J E 2004;15:427–38. doi:10.1140/epje/i2004-10061-9.
- [89] Li T, Donadio D, Galli G. Ice nucleation at the nanoscale probes no man's land of water. Nat Commun 2013;4:1887. doi:10.1038/ncomms2918.
- [90] Ajaev VS, Davis SH. The effect of tri-junction conditions in droplet solidification. J Cryst Growth 2004;264:452–62. doi:10.1016/j.jcrysgro.2003.11.119.
- [91] Marín a. G, Enríquez OR, Brunet P, Colinet P, Snoeijer JH. Universality of tip singularity formation in freezing water drops. Phys Rev Lett 2014;113:1–5. doi:10.1103/PhysRevLett.113.054301.
- [92] Yao Y, Li C, Tao Z, Yang R, Zhang H. Experimental and numerical study on the impact and freezing process of a water droplet on a cold surface. Appl Therm Eng 2018;137:83–

- 92. doi:10.1016/j.applthermaleng.2018.03.057.
- [93] Whitaker S. Forced convection heat transfer correlations for flow in pipes, past flat plates, single cylinders, single spheres, and for flow in packed beds and tube bundles. AIChE J 1972;18:361–71. doi:10.1002/aic.690180219.
- [94] Ryzhkin IA, Petrenko VF. Physical Mechanisms Responsible for Ice Adhesion. J Phys Chem B 1997;101:6267–70. doi:10.1021/jp9632145.
- [95] Wilen LA, Wettlaufer JS, Elbaum M, Schick M. Dispersion-force effects in interfacial premelting of ice. Phys Rev B 1995;52:12426–33. doi:10.1103/PhysRevB.52.12426.
- [96] Chaudhury MK, Kim KH. Shear-induced adhesive failure of a rigid slab in contact with a thin confined film. Eur Phys J E 2007;23:175–83. doi:10.1140/epje/i2007-10171-x.
- [97] Urata C, Dunderdale GJ, England MW, Hozumi A. Self-lubricating organogels (SLUGs) with exceptional syneresis-induced anti-sticking properties against viscous emulsions and ices. J Mater Chem A 2015;3:12626–30. doi:10.1039/C5TA02690C.
- [98] Wang C, Fuller T, Zhang W, Wynne KJ. Thickness dependence of ice removal stress for a polydimethylsiloxane nanocomposite: Sylgard 184. Langmuir 2014;30:12819–26. doi:10.1021/la5030444.
- [99] Susoff M, Siegmann K, Pfaffenroth C, Hirayama M. Evaluation of icephobic coatings Screening of different coatings and influence of roughness. Appl Surf Sci 2013;282:870–9. doi:10.1016/j.apsusc.2013.06.073.
- [100] Kulinich SA, Farzaneh M. Ice adhesion on super-hydrophobic surfaces. Appl Surf Sci 2009;255:8153–7. doi:10.1016/j.apsusc.2009.05.033.
- [101] Brassard JD, Sarkar DK, Perron J, Audibert-Hayet A, Melot D. Nano-micro structured superhydrophobic zinc coating on steel for prevention of corrosion and ice adhesion. J Colloid Interface Sci 2014;447:240–7. doi:10.1016/j.jcis.2014.11.076.
- [102] Kulinich SA, Farzaneh M. On ice-releasing properties of rough hydrophobic coatings. Cold Reg Sci Technol 2011;65:60–4. doi:10.1016/j.coldregions.2010.01.001.
- [103] Work A, Lian Y. A critical review of the measurement of ice adhesion to solid substrates. Prog Aerosp Sci 2018;98:1–26. doi:10.1016/j.paerosci.2018.03.001.
- [104] ASTM. Standard Test Method for Abrasion Resistance of Organic Coatings by the Taber Abraser. D4060-10 n.d. doi:10.1520/D4060.
- [105] Khanna AS. High-Performance Organic Coatings. 2008. doi:10.1533/9781845694739.
- [106] Rahimi H, Mozaffarinia R, Hojjati Najafabadi A. Corrosion and wear resistance characterization of environmentally friendly sol-gel hybrid nanocomposite coating on AA5083. J Mater Sci Technol 2013;29:603–8. doi:10.1016/j.jmst.2013.03.013.
- [107] Scrinzi E, Rossi S, Kamarchik P, Deflorian F. Evaluation of durability of nano-silica containing clear coats for automotive applications. Prog Org Coatings 2011;71:384–90. doi:10.1016/j.porgcoat.2011.04.009.
- [108] Ahmad S, Gupta AP, Sharmin E, Alam M, Pandey SK. Synthesis, characterization and development of high performance siloxane-modified epoxy paints. Prog Org Coatings 2005;54:248–55. doi:10.1016/j.porgcoat.2005.06.013.
- [109] ASTM. Standard Test Method for Film Hardness by Pencil Test. D3363-05 n.d. doi:10.1520/D3363-05R11E02.2.
- [110] ASTM. Standard Test Methods for Rating Adhesion by Tape Test. D3359-17 n.d. doi:10.1520/D3359-17.
- [111] ASTM. Standard Practice for Testing Water Resistance of Coatings in 100 % Relative Humidity. n.d. doi:10.1520/D2247-15.

- [112] ASTM. Standard Test Method for Evaluation of Painted or Coated Specimens Subjected to Corrosive Environments. D1654-08 n.d. doi:10.1016/j.snb.2011.06.074.
- [113] ASTM. Standard Practice for Operating Fluorescent Ultraviolet (UV) Lamp Apparatus for Exposure of Nonmetallic Materials. G154-16 n.d. doi:10.1520/G0154-16.2.
- [114] Subramanyam SB, Rykaczewski K, Varanasi KK. Ice adhesion on lubricant-impregnated textured surfaces. Langmuir 2013;29:13414–8. doi:10.1021/la402456c.
- [115] Lafuma A, Quéré D. Superhydrophobic states. Nat Mater 2003;2:457–60. doi:10.1038/nmat924.
- [116] Deng X, Mammen L, Butt H-J, Vollmer D. Candle Soot as a Template for a Transparent Robust Superamphiphobic Coating. Science (80-) 2012;335:67–70. doi:10.1126/science.1207115.
- [117] Tuteja A, Choi W, Ma M, Mabry JM, Mazzella SA, Rutledge GC, et al. Designing Superoleophobic Surfaces. Science (80-) 2007;318:1618–22. doi:10.1126/science.1148326.
- [118] Zhang Q, He M, Chen J, Wang J, Song Y, Jiang L. Anti-icing surfaces based on enhanced self-propelled jumping of condensed water microdroplets. Chem Commun 2013;49:4516–8. doi:10.1039/c3cc40592c.
- [119] Liu J, Zhu C, Liu K, Jiang Y, Song Y, Francisco JS, et al. Distinct ice patterns on solid surfaces with various wettabilities. Proc Natl Acad Sci 2017;114:201712829. doi:10.1073/pnas.1712829114.
- [120] Herminghaus S. Roughness-induced non-wetting. Eur Lett 2000;52:165–70.
- [121] Cheng YT, Rodak DE. Is the lotus leaf superhydrophobic? Appl Phys Lett 2005;86:1–3. doi:10.1063/1.1895487.
- [122] Gam S, Pinson J, Lamouri A, Decorse P, Bellynck S, Herbaut R, et al. Micro-patterned anti-icing coatings with dual hydrophobic/hydrophilic properties. J Mater Chem A 2018:19353–7. doi:10.1039/C8TA06944A.
- [123] Miljkovic N, Enright R, Wang EN. Liquid Freezing Dynamics on Hydrophobic and Superhydrophobic Surfaces. Trans ASME 2012;134:080902. doi:10.1016/S0040-6090.
- [124] Miljkovic N, Preston DJ, Wang EN, Enright R. Ostwald Ripening During Freezing on Scalable Superhydrophobic Surfaces. J Heat Transfer 2014;136:080901. doi:10.1109/ICASSP.2006.1659961.
- [125] Chavan S, Carpenter J, Nallapaneni M, Chen JY, Miljkovic N. Bulk water freezing dynamics on superhydrophobic surfaces. Appl Phys Lett 2017;110. doi:10.1063/1.4974296.
- [126] Pruppacher HR, Klett JD. Microphysics of Clouds and Precipitation. Dordrecht, The Netherlands: Kluwer Academic Publishers; 1997.
- [127] Wood GR, Walton AG. Homogeneous nucleation Kinetics of Ice Water. J Appl Phys 1970;41:3027–36.
- [128] Mossop SC. The Freezing of Supercooled Water. Proc Phys Soc Sect B 1954;4:193–208. doi:10.1088/0370-1301/66/3/311.
- [129] Chen J, Liu J, He M, Li K, Cui D, Zhang Q, et al. Superhydrophobic surfaces cannot reduce ice adhesion. Appl Phys Lett 2012;101:2010–3. doi:10.1063/1.4752436.
- [130] Petrenko VF, Peng S. Reduction of ice adhesion to metal by using self-assembling monolayers (SAMs). Can J Phys 2003;81:387–93. doi:10.1139/p03-014.
- [131] Chen J, Luo Z, Fan Q, Lv J, Wang J. Anti-Ice coating inspired by ice skating. Small 2014;10:4693–9. doi:10.1002/smll.201401557.

- [132] Zou M, Beckford S, Wei R, Ellis C, Hatton G, Miller MA. Effects of surface roughness and energy on ice adhesion strength. Appl Surf Sci 2011;257:3786–92. doi:10.1016/j.apsusc.2010.11.149.
- [133] Dou R, Chen J, Zhang Y, Wang X, Cui D, Song Y, et al. Anti-icing coating with an aqueous lubricating layer. ACS Appl Mater Interfaces 2014;6:6998–7003. doi:10.1021/am501252u.
- [134] Tarquini S, Antonini C, Amirfazli A, Marengo M, Palacios J. Investigation of ice shedding properties of superhydrophobic coatings on helicopter blades. Cold Reg Sci Technol 2014;100:50–8. doi:10.1016/j.coldregions.2013.12.009.
- [135] Janjua ZA, Turnbull B, Choy KL, Pandis C, Liu J, Hou X, et al. Performance and durability tests of smart icephobic coatings to reduce ice adhesion. Appl Surf Sci 2017;407:555–64. doi:10.1016/j.apsusc.2017.02.206.
- [136] Bharathidasan T, Kumar SV, Bobji MS, Chakradhar RPS, Basu BJ. Effect of wettability and surface roughness on ice-adhesion strength of hydrophilic, hydrophobic and superhydrophobic surfaces. Appl Surf Sci 2014;314:241–50. doi:10.1016/j.apsusc.2014.06.101.
- [137] Sojoudi H, Arabnejad H, Raiyan A, Shirazi SA, McKinley GH, Gleason KK. Scalable and durable polymeric icephobic and hydrate-phobic coatings. Soft Matter 2018;14:3443–54. doi:10.1039/c8sm00225h.
- [138] Sojoudi H, McKinley GH, Gleason KK. Linker-free grafting of fluorinated polymeric cross-linked network bilayers for durable reduction of ice adhesion. Mater Horiz 2015;2:91–9. doi:10.1039/C4MH00162A.
- [139] Bohn HF, Federle W. Insect aquaplaning: Nepenthes pitcher plants capture prey with the peristome, a fully wettable water-lubricated anisotropic surface. Proc Natl Acad Sci U S A 2004;101:14138–43. doi:10.1073/pnas.0405885101.
- [140] Wilson PW, Lu W, Xu H, Kim P, Kreder MJ, Alvarenga J, et al. Inhibition of ice nucleation by slippery liquid-infused porous surfaces (SLIPS). Phys Chem Chem Phys 2013;15:581–5. doi:10.1039/c2cp43586a.
- [141] Smith JD, Dhiman R, Anand S, Reza-Garduno E, Cohen RE, McKinley GH, et al. Droplet mobility on lubricant-impregnated surfaces. Soft Matter 2013;9:1772. doi:10.1039/c2sm27032c.
- [142] Kreder MJ, Alvarenga J, Kim P, Aizenberg J. Design of anti-icing surfaces: smooth, textured or slippery? Nat Rev Mater 2016;1:15003. doi:10.1038/natrevmats.2015.3.
- [143] Kim P, Wong TS, Alvarenga J, Kreder MJ, Adorno-Martinez WE, Aizenberg J. Liquid-infused nanostructured surfaces with extreme anti-ice and anti-frost performance. ACS Nano 2012;6:6569–77. doi:10.1021/nn302310q.
- [144] Jin S, Liu J, Lv J, Wu S, Wang(s) J. Interfacial Materials for Anti-Icing: Beyond Superhydrophobic Surfaces. Chem An Asian J 2018;13:1406–14. doi:10.1002/asia.201800241.
- [145] Stamatopoulos C, Hemrle J, Wang D, Poulikakos D. Exceptional Anti-Icing Performance of Self-Impregnating Slippery Surfaces. ACS Appl Mater Interfaces 2017;9:10233–42. doi:10.1021/acsami.7b00186.
- [146] Zhang G, Zhang Q, Cheng T, Zhan X, Chen F. Polyols-Infused Slippery Surfaces Based on Magnetic Fe3O4-Functionalized Polymer Hybrids for Enhanced Multifunctional Anti-Icing and Deicing Properties. Langmuir 2018;34:4052–8. doi:10.1021/acs.langmuir.8b00286.

- [147] Wang N, Xiong D, Lu Y, Pan S, Wang K, Deng Y, et al. Design and Fabrication of the Lyophobic Slippery Surface and Its Application in Anti-Icing. J Phys Chem C 2016;120:11054–9. doi:10.1021/acs.jpcc.6b04778.
- [148] Stone H a. Ice-phobic surfaces that are wet. ACS Nano 2012;6:6536–40. doi:10.1021/nn303372q.
- [149] Lv J, Song Y, Jiang L, Wang J. Bio-inspired strategies for anti-icing. ACS Nano 2014;8:3152–69. doi:10.1021/nn406522n.
- [150] Liu Q, Yang Y, Huang M, Zhou Y, Liu Y, Liang X. Durability of a lubricant-infused Electrospray Silicon Rubber surface as an anti-icing coating. Appl Surf Sci 2015;346:68–76. doi:10.1016/j.apsusc.2015.02.051.
- [151] Zhu L, Xue J, Wang Y, Chen Q, Ding J, Wang Q. Ice-phobic coatings based on siliconoil-infused polydimethylsiloxane. ACS Appl Mater Interfaces 2013;5:4053–62. doi:10.1021/am400704z.
- [152] Howell C, Vu TL, Johnson CP, Hou X, Ahanotu O, Alvarenga J, et al. Stability of surface-immobilized lubricant interfaces under flow. Chem Mater 2015;27:1792–800. doi:10.1021/cm504652g.
- [153] Wexler JS, Jacobi I, Stone HA. Shear-driven failure of liquid-infused surfaces. Phys Rev Lett 2015;114:1–5. doi:10.1103/PhysRevLett.114.168301.
- [154] Zhang S, Huang J, Cheng Y, Yang H, Chen Z, Lai Y. Bioinspired Surfaces with Superwettability for Anti-Icing and Ice-Phobic Application: Concept, Mechanism, and Design. Small 2017;13:1–20. doi:10.1002/smll.201701867.
- [155] Sun J, Wang C, Song J, Huang L, Sun Y, Liu Z, et al. Multi-functional application of oil-infused slippery Al surface: from anti-icing to corrosion resistance. J Mater Sci 2018;53:16099–109. doi:10.1007/s10853-018-2760-z.
- [156] Liu Y, Wexler JS, Schönecker C, Stone HA. Effect of viscosity ratio on the shear-driven failure of liquid-infused surfaces. Phys Rev Fluids 2016;1:1–16. doi:10.1103/PhysRevFluids.1.074003.
- [157] Jacobi I, Wexler JS, Stone HA. Overflow cascades in liquid-infused substrates. Phys Fluids 2015;27. doi:10.1063/1.4927538.
- [158] Kim JH, Rothstein JP. Delayed lubricant depletion on liquid-infused randomly rough surfaces. Exp Fluids 2016;57:1–9. doi:10.1007/s00348-016-2171-3.
- [159] Fletcher NH. Surface structure of water and ice. Philos Mag 1962;7:255–69. doi:10.1080/14786436208211860.
- [160] Fletcher NH. Surface structure of water and ice II. A Revised Model. Philos Mag 1968;18:1287–300. doi:10.1080/14786436808227758.
- [161] Ryzhkin I, Petrenko V. Violation of ice rules near the surface: A theory for the quasiliquid layer. Phys Rev B 2001;65:1–4. doi:10.1103/PhysRevB.65.012205.
- [162] Jellinek HH. Liquid-like (transition) layer on ice. J Colloid Interface Sci 1967;25:192–205. doi:10.1016/0021-9797(67)90022-7.
- [163] Rosenberg R. Why is Ice Slippery? Phys Today 2005;December:50–5. doi:10.1063/1.2169444.
- [164] Wang T, Zheng Y, Raji ARO, Li Y, Sikkema WKA, Tour JM. Passive Anti-Icing and Active Deicing Films. ACS Appl Mater Interfaces 2016;8:14169–73. doi:10.1021/acsami.6b03060.
- [165] Golovin K, Kobaku SPR, Lee DH, DiLoreto ET, Mabry JM, Tuteja A. Designing durable icephobic surfaces. Sci Adv 2016;2:1–12. doi:10.1126/sciadv.1501496.

- [166] Vasileiou T, Schutzius TM, Poulikakos D. Imparting Icephobicity with Substrate Flexibility. Langmuir 2017;33:6708–18. doi:10.1021/acs.langmuir.7b01412.
- [167] Irajizad P, Al-Bayati A, Eslami B, Shafquat T, Nazari M, Jafari P, et al. Stress-localized durable icephobic surfaces. Mater Horizons 2019. doi:10.1039/C8MH01291A.
- [168] Yin X, Zhang Y, Wang D, Liu Z, Liu Y, Pei X, et al. Integration of Self-Lubrication and Near-Infrared Photothermogenesis for Excellent Anti-Icing/Deicing Performance. Adv Funct Mater 2015;25:4237–45. doi:10.1002/adfm.201501101.
- [169] Sun X, Damle VG, Liu S, Rykaczewski K. Bioinspired Stimuli-Responsive and Antifreeze-Secreting Anti-Icing Coatings. Adv Mater Interfaces 2015;2:25–7. doi:10.1002/admi.201400479.

Table 1: Parameters of standard procedure for ice adhesion measurements.

Shear rate	а	h	l
0.1 mms ⁻¹	15 mm	300 μm	3 mm

Table 2: Standard methods to assess durability of icephobic surfaces

Test	Standard	Details		
Mechanical				
Abrasion	ASTM D4060	Different Loadings: 1 N with CS-10 abrader, 5 N with H-18, and 10 N with CS-17		
Hardness	ASTM D3363	Examined by a range of pencils with various hardness from 6B to 6H.		
Adhesion to Surface	ASTM D3359	After 90s, tape is peeled from the substrate with the angle of 180°.		
Icing/de-icing cycle	Not available yet	Not available yet		
Chemical				
Water Resistance	ASTM D2247	Exposed to saturated vapor at temperature of 38 °C.		

Corrosion Resistance	ASTM D1654	V-shape cut on the substrate and exposed to corrosive chemical.	
Environmental			
UV Resistance	ASTM G154	2000 hrs cycling. Each cycle includes 8 hrs exposure to UV-irradiation (0.49 W/m² nm at 310 nm at 70 °C) followed by 4 hrs of condensation at 50 °C.	

Table 3: Ice adhesion on various icephobic surfaces and the measurement method

Sample	Physics	τ _{Ice} [kPa]	Test Method	Reference
Bare Steel		698±112		
PMMA		463±65		
PC		400±83		
PBMA		384±52		
PDMS (Sylgard 184)		291±44		
PEMA		510±101		Relationship between
95/5 PEMA/fluorodecyl POSS		278±93	Cuvette-encased ice	contact angle and Ice
70/30 PEMA/fluorodecyl POSS	Superhydrophobic Coating	166±44	columns (-15 °C)	adhesion. [21,22]
Tecnoflon		389±63		
95/5 Tecnoflon/fluorodecyl POSS		328±97		
70/30 Tecnoflon/fluorodecyl POSS	Superhydrophobic Coating	205±40		
fluorodecyl POSS		250±54		
100/0 PDMS/Silicone Oil		62		
85/15 PDMS/Silicone Oil		77		
70/30 PDMS/Silicone Oil	PDMS Coating	41		
55/45 PDMS/Silicone Oil		33		
50/50 PDMS/Silicone Oil				
		34		
Bare steel		617		
Silicone functionalized steel		127	Centrifugal	
Nano-micro structured hydrophilic Zn-surface		816	adhesion test (CAT)	[101,102,151]
Silicone functionalized-Zn surface		98		
Etched Al/ODTMS		90		
TiO2–Zonyl (Spin coated)	Superhydrophobic Coating	175		
TiO2–Zonyl (Sprayed)		370		
MAGSS	Liquid-Liquid Interface	0.002	Surface Tilting	[81]
Bare Steel		1021		
Bare Si		1131		
pDVB on Si		852		
pPFD on Si		284	Cuvette-encased ice	Term BL is a linker-
BL (10 nm) on Si		183	columns (-15 °C)	free grafted bilayer of
BL (40 nm) on Si	Linker-free Grafting	247		pDVB/pPFDA [138]
BL (10 nm) on Steel		152		
BL (40 nm) on Steel	1	199	1	
Sylgard 184 (SG 184) 10:1		264		
SG 184 1:1		14		
	Interferial Climan	14	Shear-based (Mode	Represented samples
SG 184 10:1 + 25% 100-cP Silicone Oil	Interfacial Slippage	35	II) ice adhesion test.	are chosen. [165]
SG 184 10:1 + 25% PMHS		10		

		ı		
1:9 SG 527:184 + 25% 100-cP Silicone Oil		14		
Perfluoropolyether (PFPE)		238		
PFPE + 25% Krytox 100		31		
VytaFlex40 + 20% Vegetable Oil	Interfacial Slippage	10.5		
VytaFlex40 + 15% Cod Liver	interfacial Shippage	27		
VytaFlex40 + 10% 100-cP SO		41		
VytaFlex40 + 15% Safflower Oil		4		
VytaFlex40 + 20% Cod Liver		97		
Pure and Smooth PDMS Film				
(SF)	Photothermal Icephobic	750	Cuvette-encased ice	54.607
Porous Film (PF)	Film	2380	columns (-15 °C)	[168]
Fluorinated Porous Film (FF)		100		
PDMS resin		74.1		
AR20	Syneresis Liquid Layer	3.1	Cuvette-encased ice	[97]
AR20+TSF437	1	0.4	columns (-15 °C)	[>,]
SLWL Surface	Self-lubricating Water	67.0	Cuvette-encased ice	50.73
	Layer	67±8	columns (-15 °C)	[27]
HA-D		(Cuvette-encased ice	F1017
	Aqueous Lubricating Layer	77.6	columns (-15 °C)	[131]
PU-0		253		The number
PU-3		92	Cuvette-encased ice	represents wt% of
PU-6	Aqueous Lubricating Layer	39	columns (-15 °C)	DMPA in the
PU-9		27	columns (-13 C)	polymer particles.
				[133]
Superhydrophobic Surface		50-100		
Solid-Gel Coating with		75		
Perfluorinated Polyether	Smooth & Structured		Cuvette-encased ice	[142]
SLIPS	Surfaces/ Lubricants	15	columns (-15 °C)	[]
Lubricant-Infused Surfaces		10-100		
PDMS Mixed with Silicone Oil		1.7		
Aluminum (Al)		1070±210		
K100-A1	Liquid-infused	1145±310	Cylindrical cuvette-	
K100-F13-A1	Nanostructures	515±130	encased ice columns	[143]
F13-Ppy-Al	- Transsituation	845±52	(-20 °C)	
K100-F13-Ppy-AI (SLIPS-AI)		15.6±3.6		
S-FNM-K103		55		Reported samples
S-NM-K103	Lubricant-infused	55	Aluminum cuvette-	used to measure how
S-M-K103	Electrospray	55	encased ice columns	they will change over
S-F-K103	Diodiospiuj	55	(-20 °C)	several icing/deicing cycles. [150]



Figure 1: The importance of icephobic surfaces in a broad spectrum of systems is shown. Transportation systems, power systems, and energy systems.

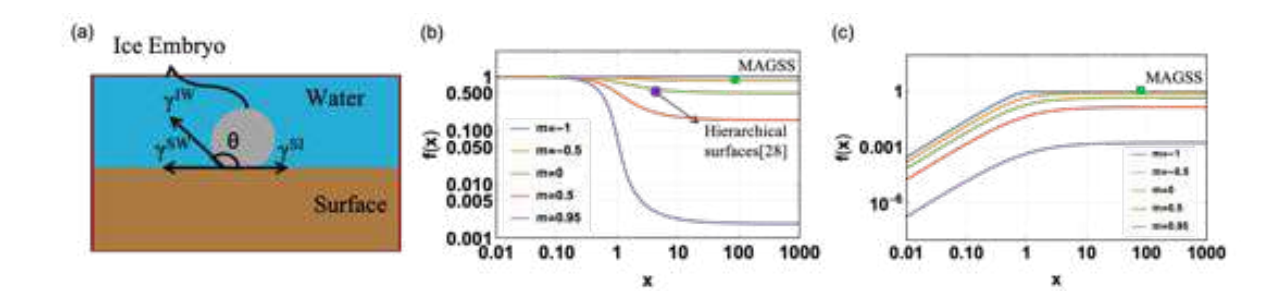


Figure 2: (a) Formation of ice nucleolus on a surface is shown in which $m = \cos \theta_{IW}$. Note that θ_{IW} is different than droplet contact angle on a surface. The surface factor is plotted for both (b) convex and (c) concave roughness on a surface. As shown, for values of x smaller than ~1, the nano-structuring can affect f(m,x) function and thus the ice nucleation temperature and ice nucleation rate. However, at higher values of x, f(m,x) function is only function of m value.

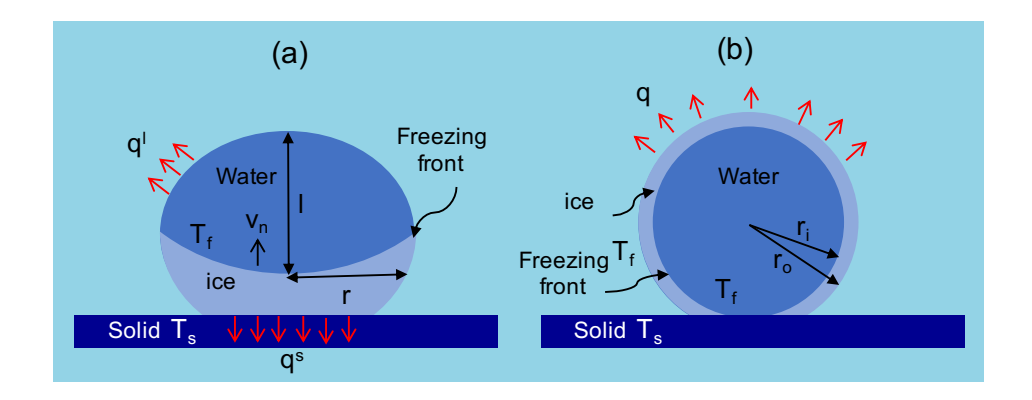


Figure 3: Schematics of ice growth on a sub-cooled surface is shown. (a) In no flow condition, the heat transfer by the solid substrate determines the ice growth rate. (b) Under a flow field, the convective heat transfer from the droplet surface determines the growth rate of the ice phase.

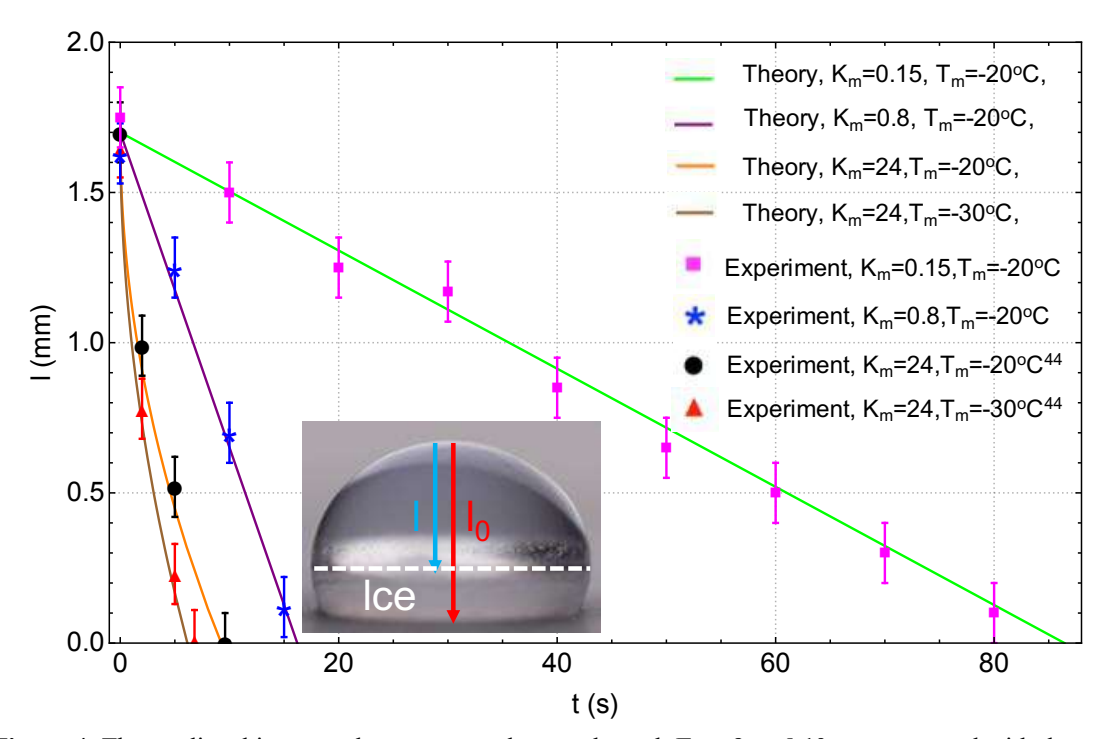


Figure 4: The predicted ice growth rates on a substrate through **Eqs. 9 and 10** are compared with the experimental data measured in this work along with the reported ones in the literature. The developed model accurately predicts ice growth dynamics.

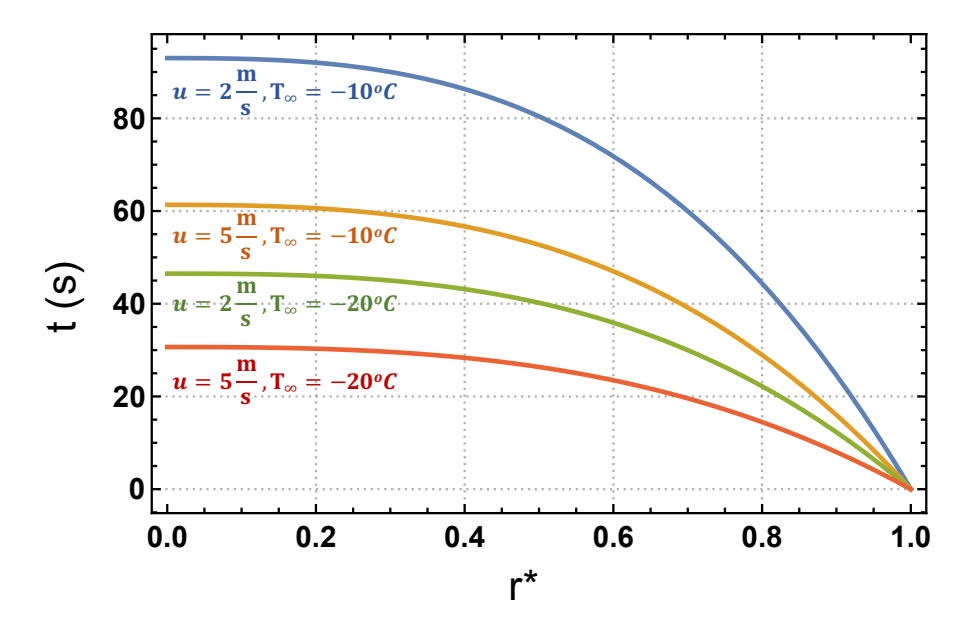


Figure 5: The predicted ice growth rates for a droplet exposed to an external flow through Eq. 14 at various wind speeds and temperatures. Note that there is no fitting parameter in the model.

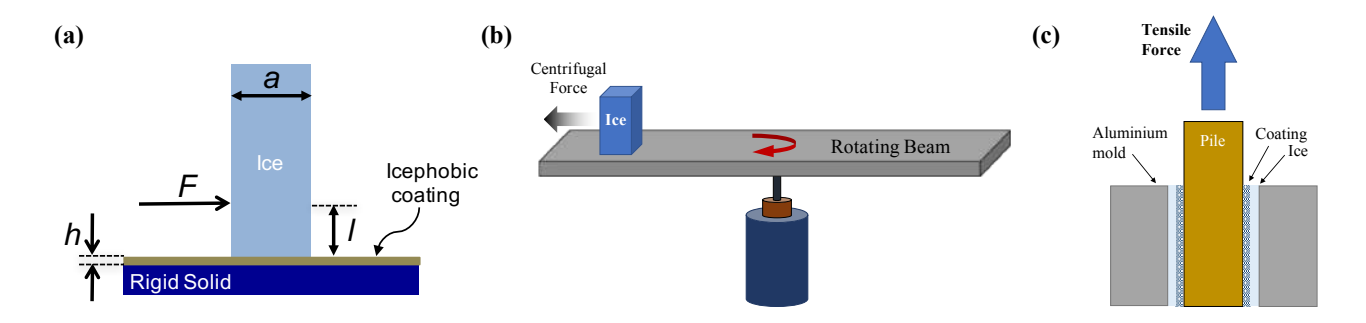


Figure 6: Schematic of the experimental approaches to measure ice adhesion. (a) Cuvette-encased ice column: shear stress for detachment of the ice column from the surface is measured. (b) Centrifugal force method: induced shear stress at the ice-coating interface through centrifugation is measured. (c) Tensile force method: induced shear stress at the interface by the tensile machine provides adhesion of ice on the coating.

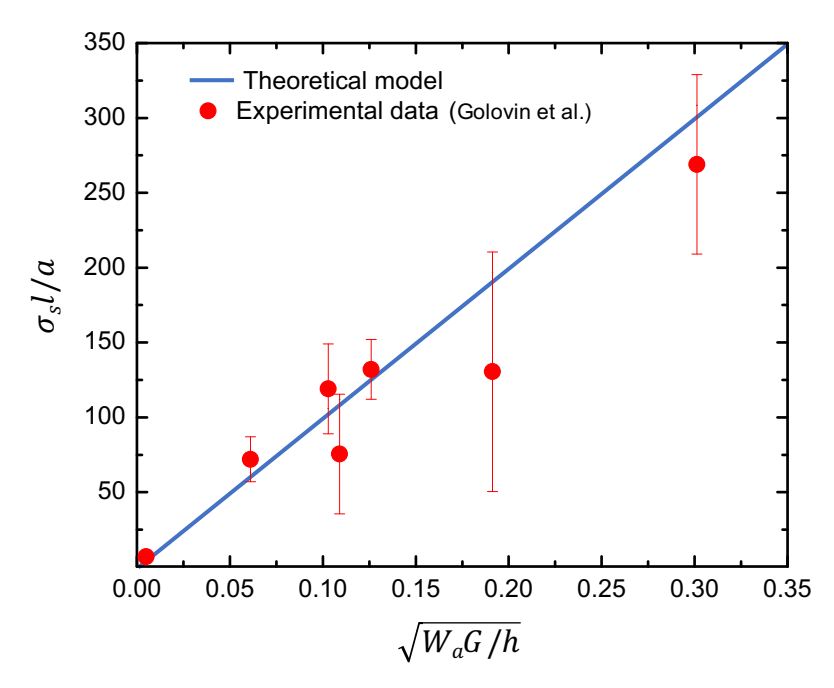


Figure 7: The reported values of ice adhesion are compared with the model in **Eq. 17**. There is a good agreement between the prediction and reported data. The high error bars is resulted from inconsistency in thickness of samples or gap between the probe and the coating (i.e. l).

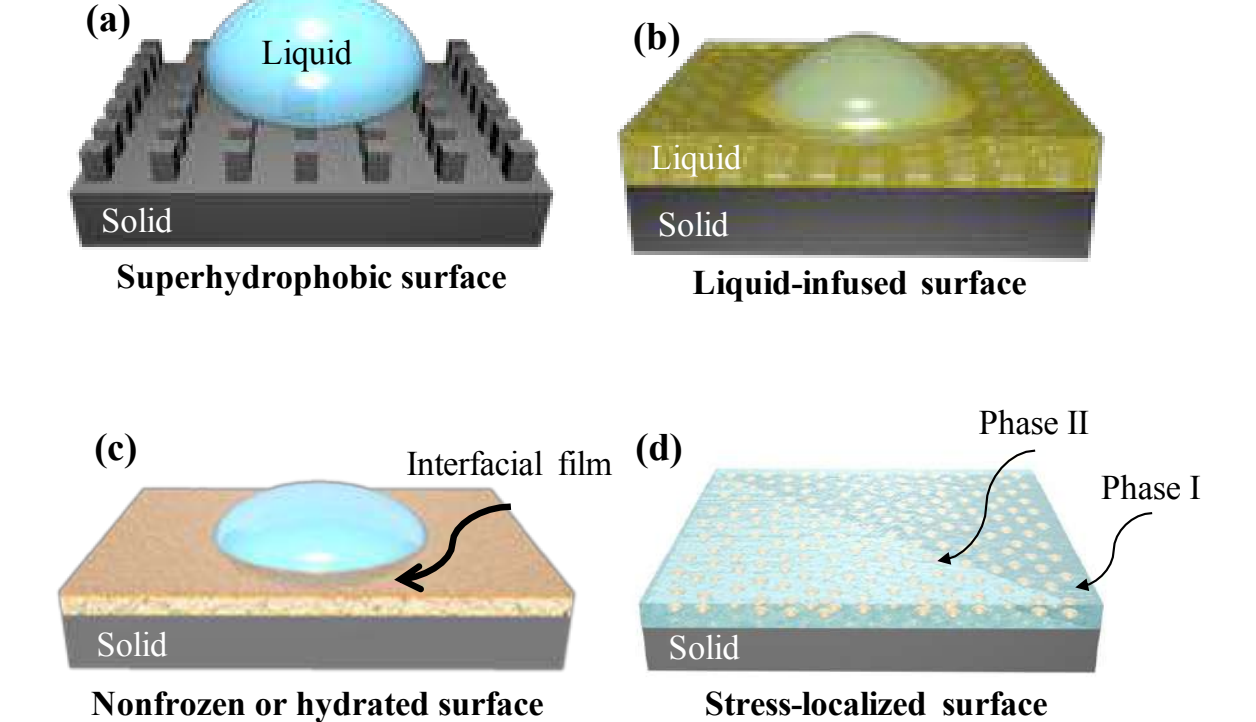


Figure 8: State-of-the-art icephobic surfaces (a) superhydrophobic surfaces, which have high ice formation temperature and high ice adhesion, (b) liquid-infused surface which show low ice adhesion, but suffer from mechanical durability, (c) hydrated and non-frozen surfaces, which show medium ice adhesion strength and their durability is not addressed yet, and (d) stress-localized surfaces that show low ice adhesion and high durability.

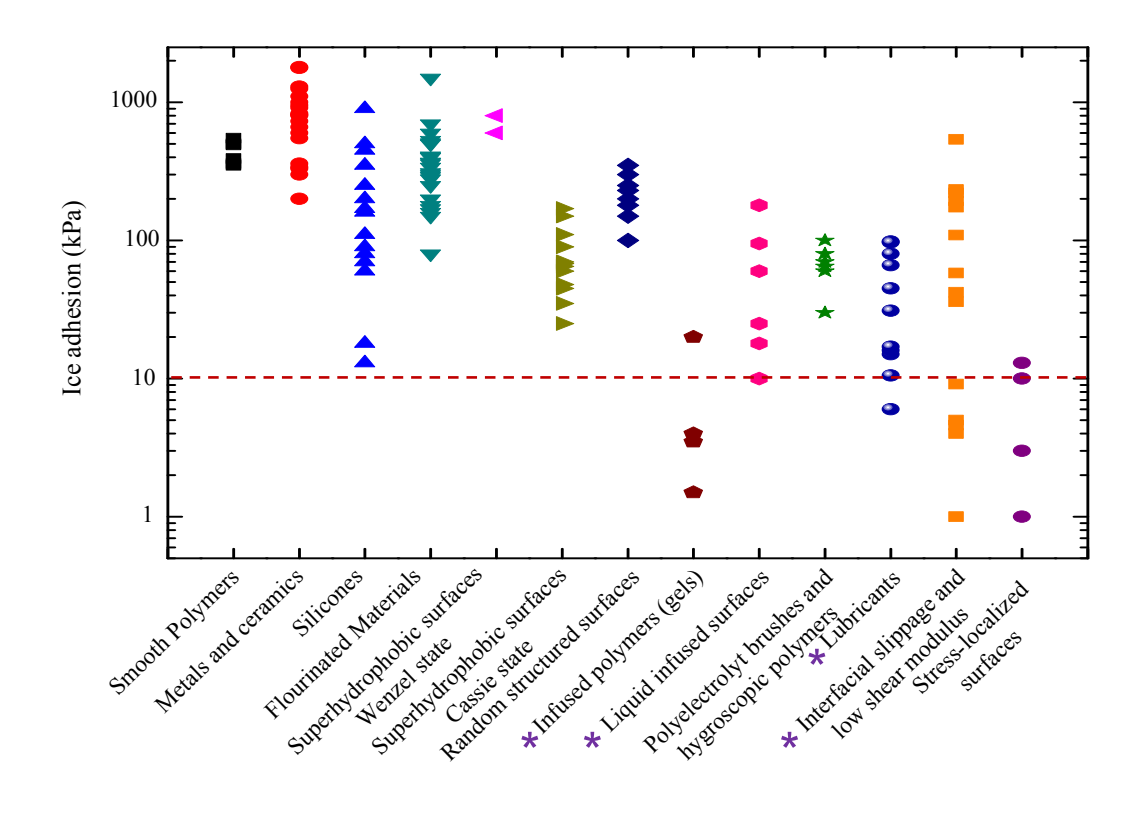


Figure 9: Ice adhesion on a wide range of studied surfaces is compared [21,22,27,36,65,81,97,131,133,138,140,142,143,150,151,165,167–169]. The materials that are marked with a star are not mechanically durable and their properties degrade after several icing/deicing cycles. In ideal passive anti-icing surfaces, ice should detach from the surface by its own weight or other natural forces such as wind shear (i.e. ice adhesion < 10 kPa).